Am J Transl Res 2022;14(6):4229-4250
www.ajtr.org /ISSN:1943-8141/AJTR0141243

Original Article

Immunological significance of prognostic markers for breast cancer based on alternative splicing

Rong Xu[1], Qinglong Yang[2]

[1]*Department of Histology and Embryology, Xiangya School of Medicine, Central South University, Changsha 410013, Hunan, China;* [2]*Department of General Surgery, Guizhou Provincial People's Hospital, Guizhou 550000, Guiyang, China*

Received December 21, 2021; Accepted April 27, 2022; Epub June 15, 2022; Published June 30, 2022

Abstract: Objectives: Breast cancer (BC) currently has the highest incidence rate. Epigenetic regulation could alter gene expression and is closely related to BC initiation. This study aimed to develop an alternative splicing (AS)-based prognostic signature and clarify its relevance to the tumor immune microenvironment (TIME) status and immunotherapy of BC. Methods: Cox regression analysis was conducted to screen for prognosis-related AS events. Thereafter, LASSO with Cox regression analyses was designed to construct a prognostic signature model. Kaplan-Meier survival analysis, receiver operating characteristic curves, and proportional hazard model were then utilized to confirm the prognostic value. Multiple methods were employed to reveal the context of TIME in BC. QPCR, western blotting and immunofluorescence microscopy were carried out to detect myc-associated zinc finger protein (MAZ) expression in different cell lines, and BC and paracancerous tissues. Results: A total of 1,787 prognosis-related AS events were screened. Eight AS prognostic signatures were constructed with robust predictive accuracy based on the splicing subtypes. Furthermore, the establishment of a quantitative prognostic nomogram and consolidated signature was significantly correlated with TIME diversity and immune checkpoint blockade-related genes. MAZ was detected to be upregulated in BC. Finally, a newly constructed splicing regulatory network model revealed the potential functions of splicing factors. Conclusions: AS-splicing factor networks may enable a new approach to investigating potential regulatory mechanisms. Moreover, pivotal players in AS events with regards to TIME and efficiency of immunotherapy were uncovered and could facilitate clinical decision-making and individual determination of BC prognosis.

Keywords: Breast cancer, alternative splicing, epigenetics, immunotherapy, immune microenvironment, prognosis

Introduction

Cancer continues to be a major health problem worldwide. It has been estimated that in 2020, approximately 19.3 million new cancer cases will be diagnosed worldwide [1]. Breast cancer (BC) recently became the most common cancer globally. According to statistics, 2,261,419 new cases of BC were diagnosed worldwide in 2020, accounting for 11.7% of the total cancer incidence. Furthermore, the number of BC deaths was 684,996, constituting 6.9% of all cancer deaths [2]. The tumor, nodes, and metastases (TNM) classification is often used to stage BC and determine its prognosis. Nonetheless, although patients with the same stage generally undergo the same treatments, they can often have completely different outcomes, indicating the need to improve the prognostic ability of TNM staging [3-5]. There are several types of BC, and different subtypes are associated with different gene mutations, thereby making it difficult to predict the biological behavior of BC [6-8].

Recently, several studies showed that the initiation and progression of BC are closely related to characteristics of the tumor immune microenvironment (TIME) [9-11]. Accordingly, immunotherapy has become a promising new field in BC treatment [12-18]. However, at present, immunotherapy for BC is still in its rudimentary stage and is not effective for all patients [19, 20].

The most effective anticancer strategy is to accurately predict the response of specific malignant tumors to immunotherapy and tumor progression. Based on molecular risk distribu-

tion, subgroups of BC patients can be identified, the prediction accuracy can be improved, and the effect of immunotherapy can be optimized.

AS is defined as the formation of mRNA splicing variants from pre-mRNA via diverse splicing processes. Ultimately, the final protein products following AS of mRNA can have different or antagonistic functional and structural properties [21-24]. AS modes mainly include an alternate acceptor site (AA), alternate promoter (AP), alternate donor site (AD), alternate terminator (AT), retained intron (RI), exon skipping (ES), and mutually exclusive exons (ME) [25]. Recently, several reports revealed that AS regulates gene expression and is involved in tumorigenesis and development, and many cancer-related genes are regulated by AS. Owing to the clear diagnostic value of cancer-specific splicing variants, research on cancer and AS has attracted a great deal of interest [26, 27]. To date, several studies have investigated the relationship between AS and the initiation, progression, and metastasis of BC [28, 29]. Nevertheless, The relationship of BC characteristics and the tumor microenvironment with immunotherapy effectiveness is still unclear, however. Hence, multifactorial investigation of AS events and in-depth exploration of the relationship between tumor immune cell infiltration, immunotherapy, and prognosis is of critical importance.

In this study, we identified AS modes of The Cancer Genome Atlas (TCGA) BRCA cohort, and we screened out survival-related AS events. Thereafter, We designed and tested AS-based prognostic signatures and created an AS-clinical nomogram that can be used in the prognosis of BC patients. Correlations of the prognostic signature with tumor microenvironment complexity and immunotherapy effectiveness were then assessed, and the potential functions of MAZ in BC were evaluated. Finally, a regulatory network model was constructed to visualize co-expression relationships between alternative splicing and splicing factors.

Materials and methods

Retrieval of transcriptomic and AS data, and differential expression analysis

We downloaded transcriptome profiling (RNA-seq) data for BC from the BRCA project of TCGA (https://tcga-data.nci.nih.gov/tcga/). The AS data of the TCGA-BRCA database were retrieved from SpliceSeq (http://bioinformatics.mdanderson.org/TCGASpliceSeq). The percent spliced in (PSI) value was set to > 0.75 as the filter endpoint, and samples were filtered. All analyses were conducted in accordance with published TCGA guidelines. **Figure 1** outlines the workflow of this study.

Preparation of the AS data

We computed the PSI and constructed an upset plot to quantify AS events and identify the seven types of AS events (AA, AD, AP, AT, ES, ME, and RI). Each splicing event was defined by combining a genetic symbol, ID number, and AS mode.

Definition of survival-associated AS events

To ensure the reliability of the results, only AS with a PSI > 0.01 was included. Univariate analysis of the screened AS data was applied to determine the relationship between AS events and overall survival (OS) (Table S1). To visualize OS-related AS events, we also generated an upset plot and volcano plot. In addition, we built a bubble chart to visually examine the top 20 AS events that were most strongly related to BC prognosis among the seven AS modes.

Establishment of the prognostic model

First, LASSO regression was used to delete a high-correlation AS event in order to avoid overfitting in the model. After that, a prognostic model was constructed via multivariate Cox analysis of the screened AS events. By means of the created model, the risk score value of each patient could be obtained. The formula for quantification of the risk score was: Risk score = βAS event 1 × PSIAS event 1 + βAS event 2 × PSIAS event 2 + ⋯ + βAS event n × PSIAS event n.

Validation of the prognostic model

Kaplan-Meier analysis was applied to verify the cut-off point to assess the difference between low-risk and high-risk BC patients. Next, to verify the prognostic ability of the model, we plotted the survival curve, risk heatmap, risk curve, survival status chart, and time-dependent receiver operating characteristic (ROC) curves [30]. Univariate and multivari-

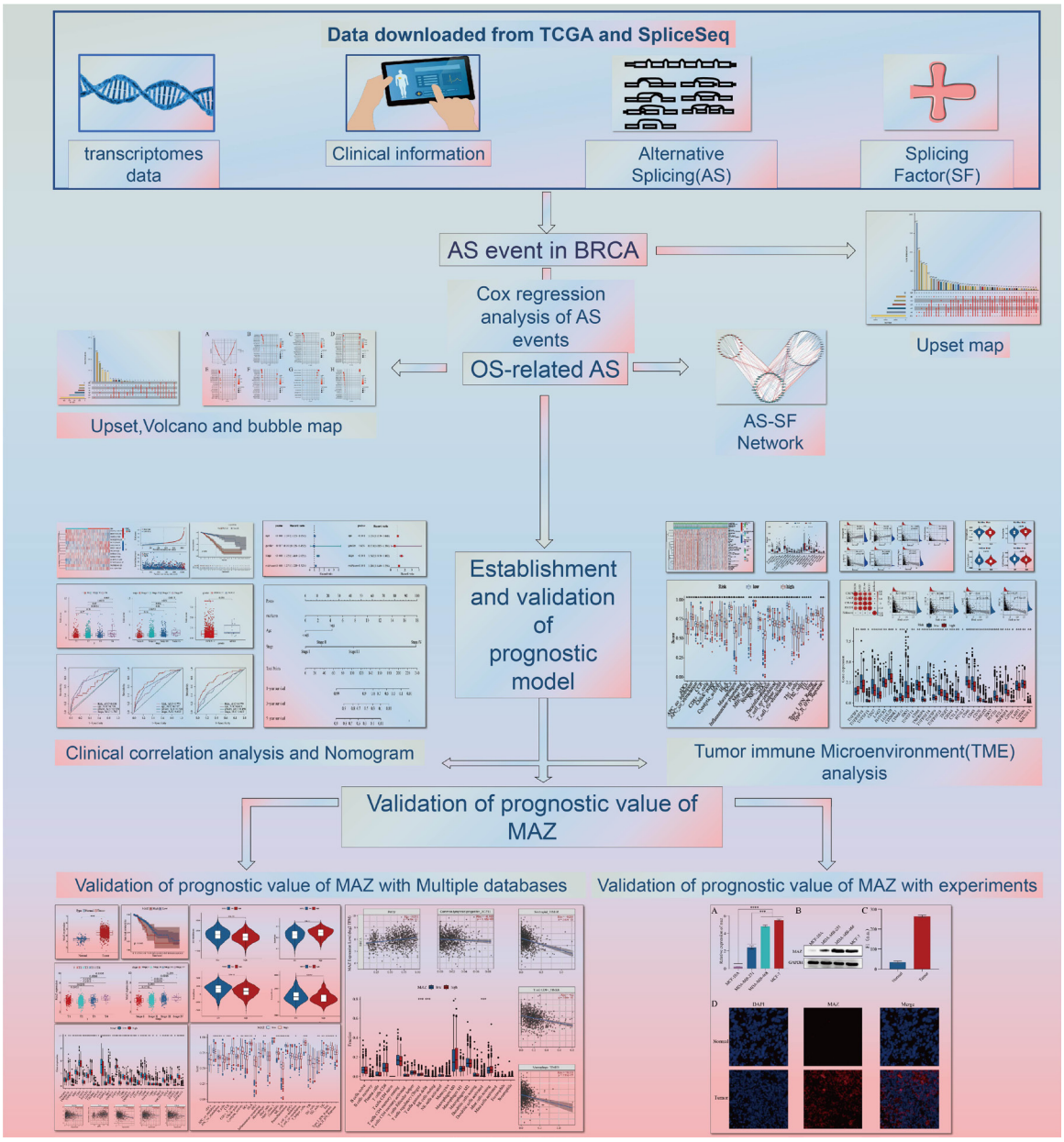

Figure 1. General research design. Flowcharts illustrate the frame of analysis.

ate Cox regression analyses were also performed on the risk score versus clinical parameters to verify whether the model can be considered an independent predictive factor for clinical prognosis. Furthermore, in the clinical correlation analysis, we determined whether there were differences between different clinical traits and stages of the same clinical characteristics. The following R packages were used for this analysis: ggplot2, glmnet, pbapply, survival ROC, survminer, and pHeatmap.

Construction of the prognostic nomogram

To comprehensively evaluate the prognostic ability of the prognostic model, by means of tumor stage, sex, and age for 1-, 3-, and 5-year OS, we generated ROC curves to calculate the area under the curve values. To quantify the impact of various clinical parameters on the prognosis of each BC patient, we developed a nomogram. We then calculated the concordance index and used this value to define the model prognostic value.

Analysis of correlation between the tumor immune microenvironment and the risk score

Tumor immune cell infiltration data were retrieved from the Tumor Immune Estimation Resource (TIMER) (https://cistr ome.shinyapps.io/timer/). The correlation between tumor immune cell infiltration and the prognostic risk score was then determined. After the downloaded data were evaluated by correlation analysis, the Stromal Score (reflects the sum of stromal and immune cells), Immune Score (reflecting the number of immune cells), ESTIMATE Score (reflects the sum), and Tumor Purity (reflecting the purity of the tumor) of each sample were obtained. The data were combined with the newly developed prognostic model, and thus, differences in scores between the high- and low-risk groups of BC patients were determined and the results visualized. Data on the percentage of infiltration of each tumor specimen by each immune cell subtype were downloaded from CIBERSORT (https://cibersort.stanford.edu/). We performed single-sample gene set enrichment analysis (ssGSEA) to clarify the enrichment of two different risk groups in the immune function-related gene set. The following R packages were utilized in the above process: limma, estimate, ggpubr, and GSEAbase.

Analysis of correlation between risk scores and immune checkpoints

According to the currently available evidence, immune checkpoint inhibitors are effective in the treatment of BC [31]. Thus, we focused on four key immune checkpoints [tumor necrosis factor superfamily receptor 5 (TNFRSF5, also known as CD40), CD200 receptor 1 (CD200R1), hepatitis A virus cellular receptor 2 (HAVCR2, also called TIM3), and leukocyte associated immunoglobulin-like receptor 2 (LAIR2)], which are considered to be key immune checkpoint proteins in BC [32-36], to investigate whether the constructed prognostic model can assess the efficacy of immune checkpoint inhibitors. Next, we sought to assess differential expression of multiple immune checkpoints in the high-risk group compared with the low-risk group.

Construction of a model of the AS-splicing factor regulatory network

Based on previous studies, 404 splicing factors (SFs; Table S2) and the RNA sequence data for the SFs were retrieved from TCGA [37]. We conducted a correlation analysis to estimate associations between the SFs and OS-related AS events (Table S3). The *p*-value filter was set to 0.001, and the correlation coefficient filter was set to 0.6. To visualize the relationships between SFs and AS, we constructed an -SF-AS regulatory network model in Cytoscape (version 3.6.1).

Cell culture

MCF-10A cells (human normal breast epithelial cells) and three human BC cell lines (MDA-MB-231, MCF-7, and MDA-MB-468) from the Shanghai Institute of Biochemistry and Cell Biology were cultured in DMEM containing 10% of FBS (Invitrogen, Carlsbad, CA, USA). Cells were cultured at 37°C in a humidified atmosphere containing 5% CO_2 at 99% relative humidity.

RNA isolation and quantitative reverse-transcription PCR (qRT–PCR)

Total RNA was extracted using TRIzol™ reagent (Invitrogen, Carlsbad, CA, USA). Reverse transcription was carried out with a reverse transcription kit (Vazyme, Nanjing, China). The cDNA was subjected to qRT-PCR using SYBR Green qPCR Master Mix (Takara) on an Applied Biosystems 7500/7500 Fast Real-Time PCR System to detect the mRNA level of *MAZ*. Experiments were carried out in triplicate. *GAPDH* served as the control gene, and expression of *MAZ* was calculated by the $2^{-\Delta\Delta Ct}$ method. The primers sequences for the qPCR were: *MAZ*, 5'-TGCCTTGGAGAAGAAGACAAAGAGC-3' (forward) and 5'-GCTTGTGTCGGTTCAGGTGGTAG-3' (reverse); and *GAPDH*, 5'-GTGAACCATGAGAAGTATG-3' (forward) and 5'-CGGCCATCACGCCACAGTTTC-3' (reverse).

Western blotting and immunofluorescence staining

The protein levels of MAZ were determined by western blotting. Anti-MAZ antibodies (ab85-725 and ab221464) were used to detect the protein bands of MAZ, as previously described. Tissues were stained with an anti-MAZ antibody as well as the nuclear stain DAPI. Normal and tumor tissues were examined and imaged by means of a fluorescence microscope.

Table 1. Baseline data of all C patients

Characteristic	Type	N	Proportion (%)
Age	≤ 65	768	70.71823204
	> 65	318	29.28176796
gender	female	1074	98.89502762
	male	12	1.104972376
stage	I	183	16.85082873
	II	621	57.18232044
	III	249	22.9281768
	IV	20	1.841620626

Statistical analysis

The Wilcoxon test was used to analyze the expression of immune checkpoints and MAZ in BC tissues and normal tissues. The Kruskal-Wallis test was carried out to compare the expression of MAZ in MCF-10A and BC cells. Kaplan-Meier analysis was applied to verify the survival of low-risk and high-risk BC patients. Univariate and multivariate Cox regression analyses were also performed to analyze the hazard, and asses the prognostic factors of survival. Pearson's correlation analysis was performed to determine the differences between clinical traits and stages of clinical characteristics. $P < 0.05$ deemed as statistical significance. R software (version 4.0.2) was utilized for all statistical analyses.

Results

Clinical information and AS event subtype analysis in BC

The clinical data of 1,109 BC patients were obtained from TCGA database, and 23 patients were excluded from the study for incomplete clinical information. Thus, a total of 1,086 patients were analyzed. **Table 1** presents clinically relevant information about the patients. Statistical values were determined for the proportion of each subtype of AS events, and an upset plot was generated (**Figure 2A**). The results indicate that the AS modes with the highest frequency and lowest frequency were ES and ME, respectively.

Identification of the OS-related AS events

Univariate analysis was applied to analyze the downloaded AS events, and 1,781 OS-related AS events were filtered out ($P < 0.05$). The detailed results of the univariate analysis are presented in the Supplementary Materials (Table S1). To visualize the AS events related to prognosis, we reconstructed the upset plot and generated a volcano plot (**Figures 2B** and **3A**). As shown in **Figure 2B**, the AS modes with the highest frequency and lowest frequency were ES and ME, respectively. **Figure 3B-H** depict the top 20 survival-relevant subtypes of each AS mode.

Establishment of the prognostic model

We performed LASSO regression and multivariate analyses to assess the prognostic utility of AS events related to survival. The specific LASSO regression results on each subtype of AS and combined AS events are listed in **Figure 4A**, **4B** as well as in Figures S1A-G and S2A-G. To screen out the most survival-related AS, we carried out multivariate Cox regression analysis. Ultimately, eight AS-based prognostic signatures (AA, AP, AT, AD, ME, ES, RI, and ALL [combination of the above]) were compiled.

Validation of the prognostic model

The median risk score sorted BC patients into two groups (high-risk/low-risk). To test whether an AS event belongs to the high-risk or low-risk group, we plotted a risk heatmap (**Figures 4C**, S3A, S3D, S4A, S4D, S5A, S5D, S5G). The risk curve (**Figures 4D**, S3B, S3E, S4B, S4E, S5B, S5E, S5H) and survival scatter plot (**Figures 4E**, S3C, S3F, S4C, S4F, S5C, S5F, S5I) indicate that the OS of patients with low-risk was significantly better compared with that of high-risk patients. The Kaplan-Meier curve yielded the same result: high-risk patients had a worse prognosis (**Figures 4F**, S6A, S6C, S6E, S6G, S7A, S7C, and S7E; all $P < 0.001$). To further analyze the prognostic ability of the model, we plotted and analyzed ROC curves for different durations of survival (1 year, 3 years, and 5 years). The AUC at 3 and 5 years was greater than 0.75, suggesting that the model had good sensitivity and specificity (**Figures 4G**, S6B, S6D, S6F, S6H, S7B, S7D, S7F). Moreover, in an independent prognostic analysis (**Figures 4H**, **4I** and S8A-N), the model was found to be potentially independent of other clinical parameters, which is an independent prognostic factor of BC. A stratification analysis was performed to confirm that the ALL prognostic features still had a strong prognostic ability when

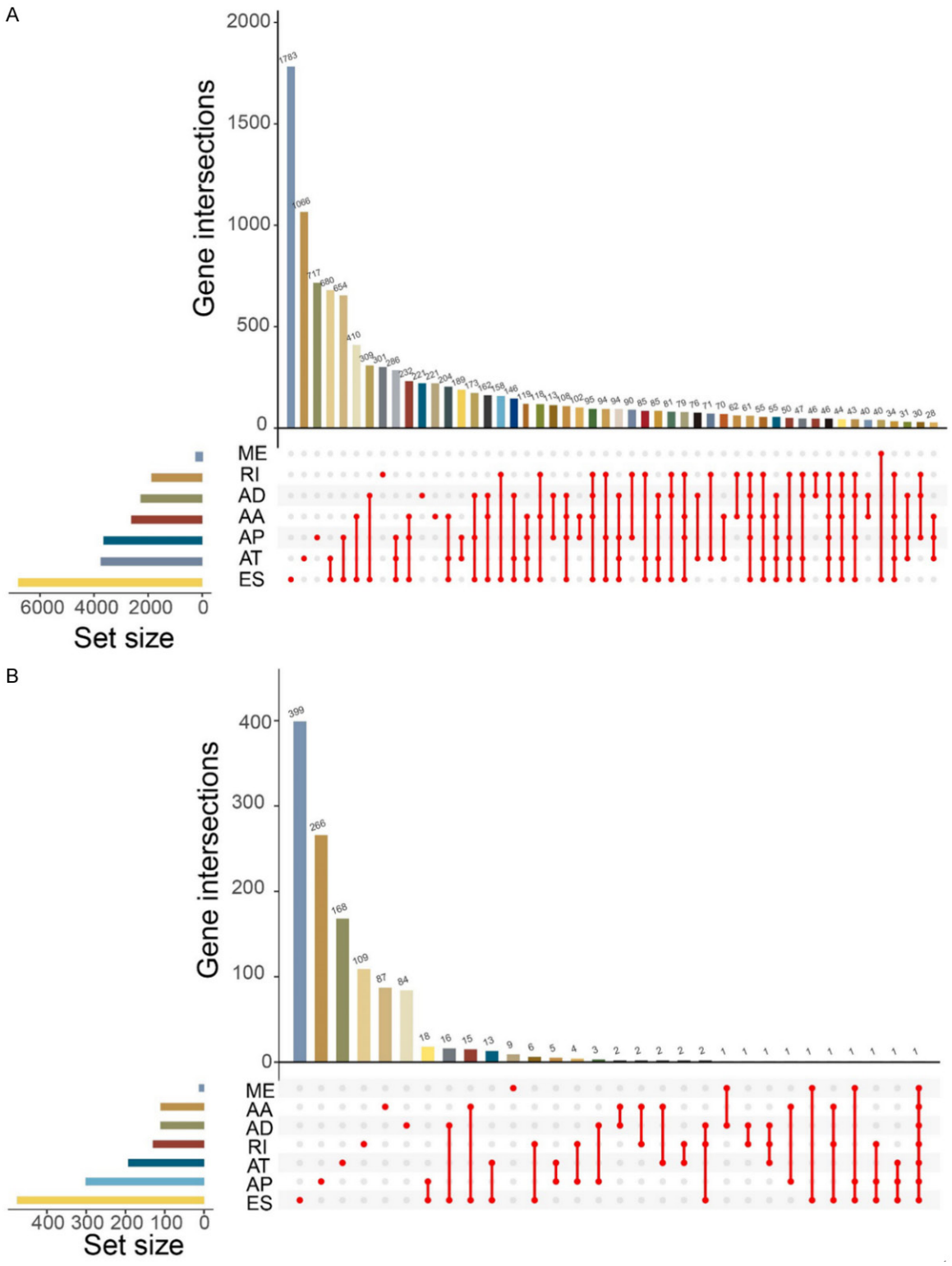

Figure 2. A. UpSet plot showing the gene interactions in AS events in TCGA BRCA cohort. B. UpSet plot showing gene interactions in survival-related AS events.

BC patients were divided into different subgroups according to the clinical characteristics. Compared to patients with low-risk values, the prognoses of high-risk BC patients in both the

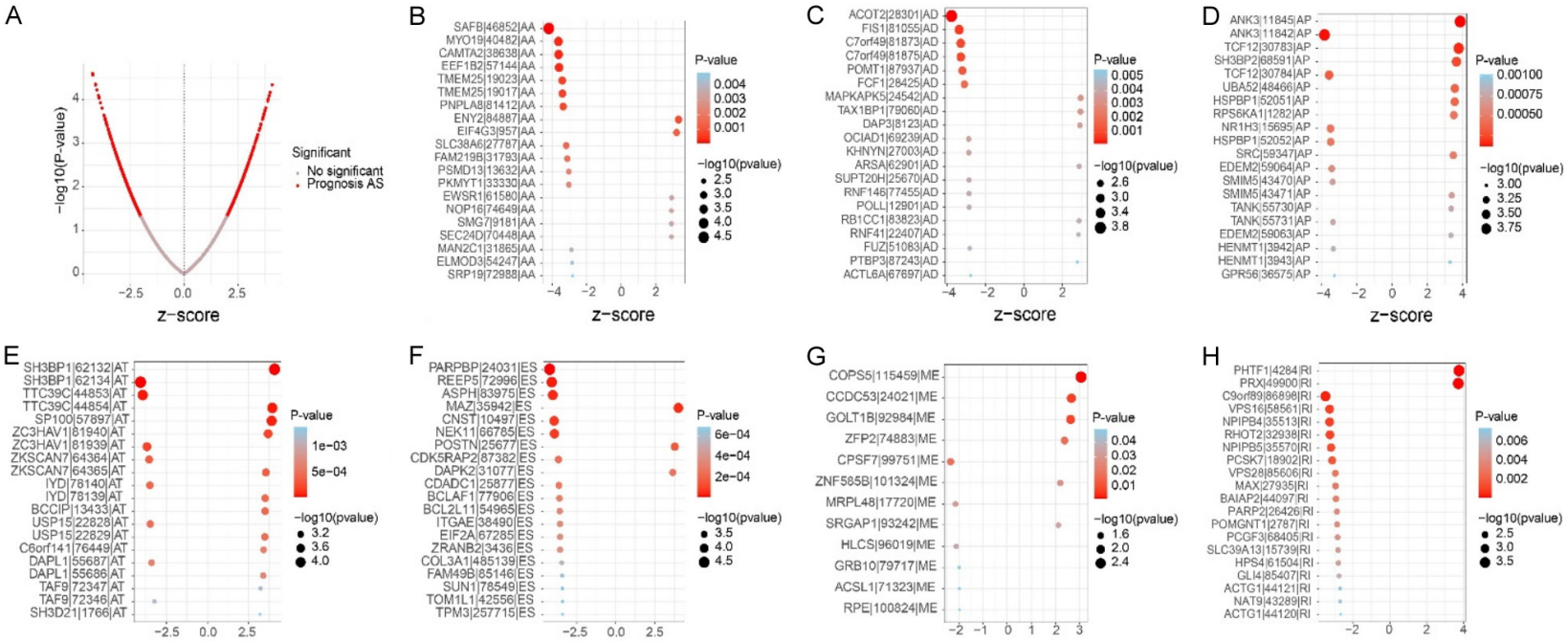

Figure 3. Survival-related AS events. A. The volcano plots show the survival-related AS events. B-H. The most important survival-related AAs, APs, ATs, ADs, MEs, ESs, and RIs in TCGA BRCA cohort.

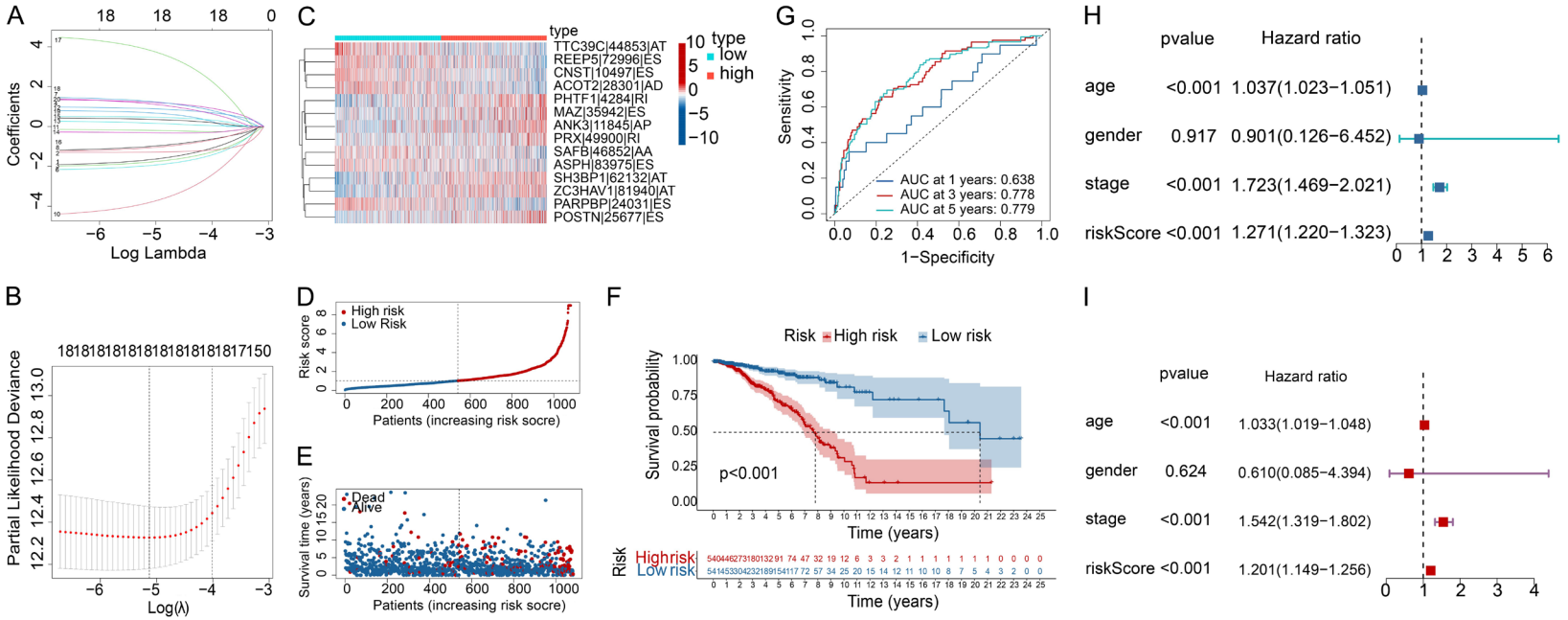

Figure 4. Confirmation of ALL AS-based prognostic features. (A) LASSO coefficient profiles in the seven types of AS events. (B) Validation of tuning parameter selection in LASSO regression. (C) Heatmap of PSI values of ALL signature in AS events. Red indicates high expression, and blue indicates low expression. (D) ALL signature risk score distribution. (E) The survival status and time of patients. (F) Kaplan-Meier survival analysis. (G) ROC analysis of overall survival prediction using risk score. The results of (H) univariate and (I) multivariate Cox regression.

early- and late-stage subgroups were poorer (Figure S9A and S9B). Similarly, patients with T1-2 or T3-4 status showed good prognostic performances in prognostic feature (Figure S9C and S9D), male or female patients (Figure S9E and S9F), patients with M0 or M1 status (Figure S9G and S9H), patients with N0, N1, N2, or N3 status (Figure S9I-L), and patients aged ≤ 58 years or > 58 years (Figure S9M and S9N). These results indicate that this signature could be a prominent prediction factor independent of the clinical parameters of BC patients.

Clinical correlation analysis and construction of the AS-clinicopathological nomogram

To test whether there were differences in patient risks between various clinical parameters, we performed a clinical correlation analysis. With the progression of BC [T stage (**Figure 5A**) and advanced clinicopathological stage (**Figure 5B**) increased], the risk score exhibited an upward trend. The results of this analysis also suggest that the risk score is a potential prognostic indicator of BC. The risk of BC did not differ between males and females (**Figure 5C**), probably owing to the small sample size for males: which was only 12 cases. To compare the prognostic ability of this model with that of other clinical parameters, we plotted ROC curves for 1-, 3-, and 5-year ROC curves (**Figure 5D-F**) and examined each curve to find the optimal AUC value. We then constructed a prognostic nomogram by combining our prognostic model and clinical characteristics with AUC > 0.6 (**Figure 5G**). The C-index of the nomogram was 0.8174151, indicating that the nomogram has a robust predictive ability.

Analysis of the correlation between the prognostic model and tumor-infiltrating immune cells

We tested the predictive power of the prognostic model in terms of immunity, and we performed an analysis of the correlation between the prognostic risk score and tumor-infiltrating immune cells from the TIMER, immune score (calculated via the ESTIMATE algorithm), ssGSEA signatures, and tumor-infiltrating immune cell subtypes and levels (calculated by the CIBERSORT method). First, the TIMER results suggest that the risk score positively correlated with M2 macrophages (r = 0.16; P = 4.8e-0.6) (**Figure 6A**) and negatively correlated with resting dendritic cells (DCs; r = -0.12; P = 0.00036), activated natural killer (NK) cells (r = -0.0097; P = 0.0049), $CD8^+$ T cells (r = -0.2, P = 8.1e-09), and regulatory T cells (Tregs; r = -0.13, P = 0.00017) (**Figure 6B-D**). Moreover, patients in the high-risk group had fewer immune and stromal infiltrating cells in the tumor and higher tumor purity than did patients in the low-risk group (**Figure 6E-H**). Assessment and visualization of the differences between the two groups (high risk/low risk), in terms of immune cells and immune cell-related functions, revealed that the degree of immune cell infiltration [B cells, $CD8^+$ T cells, T follicular helper cells, T helper 1 (Th1) cells, Th2 cells, mast cells, neutrophils, NK cells, activated DCs, all Th cells, DCs, immature DCs, plasmacytoid DCs, and tumor-infiltrating lymphocytes (TILs)] and immune cell-related activities decreased as the risk in question increased (**Figure 6G-I**). In summary, we were able to explain the indicators of poor prognosis of high-risk BC patients from the perspective of tumor immune cell infiltration.

Correlation and difference analysis between the risk score and immune checkpoint proteins

Several studies have confirmed that the initiation and progression of BC are strongly related to characteristics of the immune system [38, 39]. In light of this, there is now an abundance of well-advanced clinical research on tumor immunotherapy, especially on immune checkpoint inhibitors. Therefore, in this work, we selected what are considered to be the four most important immune checkpoint suppressor genes (*CD40*, *CD200R1*, *HAVCR2*, and *LAIR1*) in BC. First, we tested correlations among these four genes, and between them and the risk score, to determine whether the prognostic model can accurately predict the efficacy of immunotherapy (**Figure 7A**). Significant negative correlations among *CD40*, *CD200R1*, *HAVCR2*, and *LAIR1* were found (**Figure 7B-E**). Furthermore, the risk score was negatively correlated with these traditional immune checkpoint-related genes (*CD40*, [R = -0.25, P < 2.2e-16], *CD200R1* [R = -0.11, P = 0.00023], *HAVCR2* [R = -0.11, P = 0.00022], and *LAIR1* [R = -0.14, P = 2.8e-06]). In addition to the recognized immune checkpoint-related genes associated with BC, we analyzed other

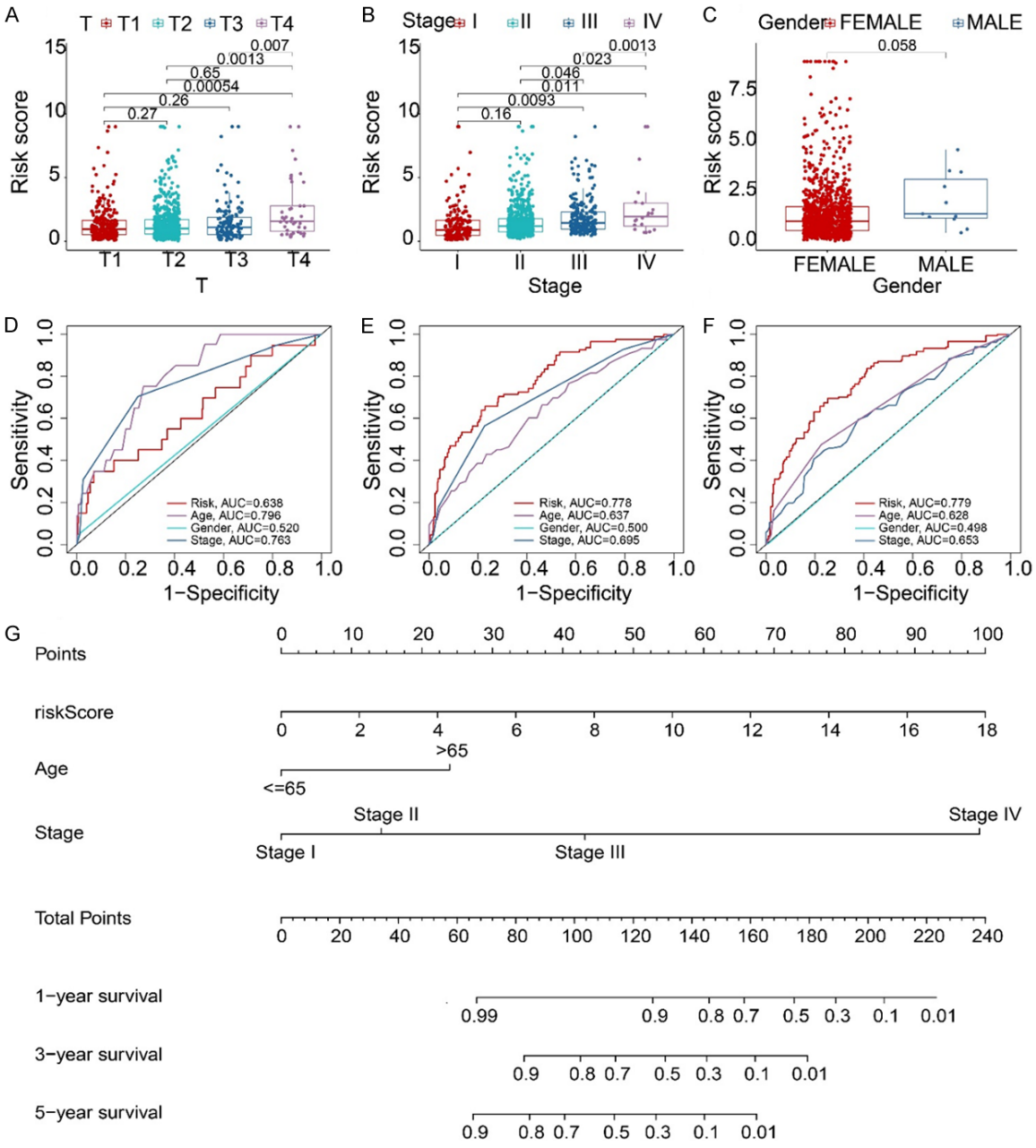

Figure 5. Correlation between ALL prognostic signature and clinical features and construction of a clinicopathological nomogram of AS. Correlation of risk score with (A) T status, (B) stage, and (C) gender. (D-F) Prediction of 1-, 3-, and 5-year survival using different clinical features. (G) Nomogram was assembled to predict survival of patients with BC.

common immune checkpoint-related genes. A total of 31 genes proved to be significantly downregulated in high-risk patients (**Figure 7F**). Overall, the prognosis of high-risk groups appeared to be poor, which may be attributed to the low expression of genes associated with immune checkpoints.

MAZ is an independent prognostic factor and is associated with the key immune checkpoint suppressor genes

MAZ is the most differentially expressed gene among the genes related to the prognosis of AS (Table S4). Therefore, we chose this gene for

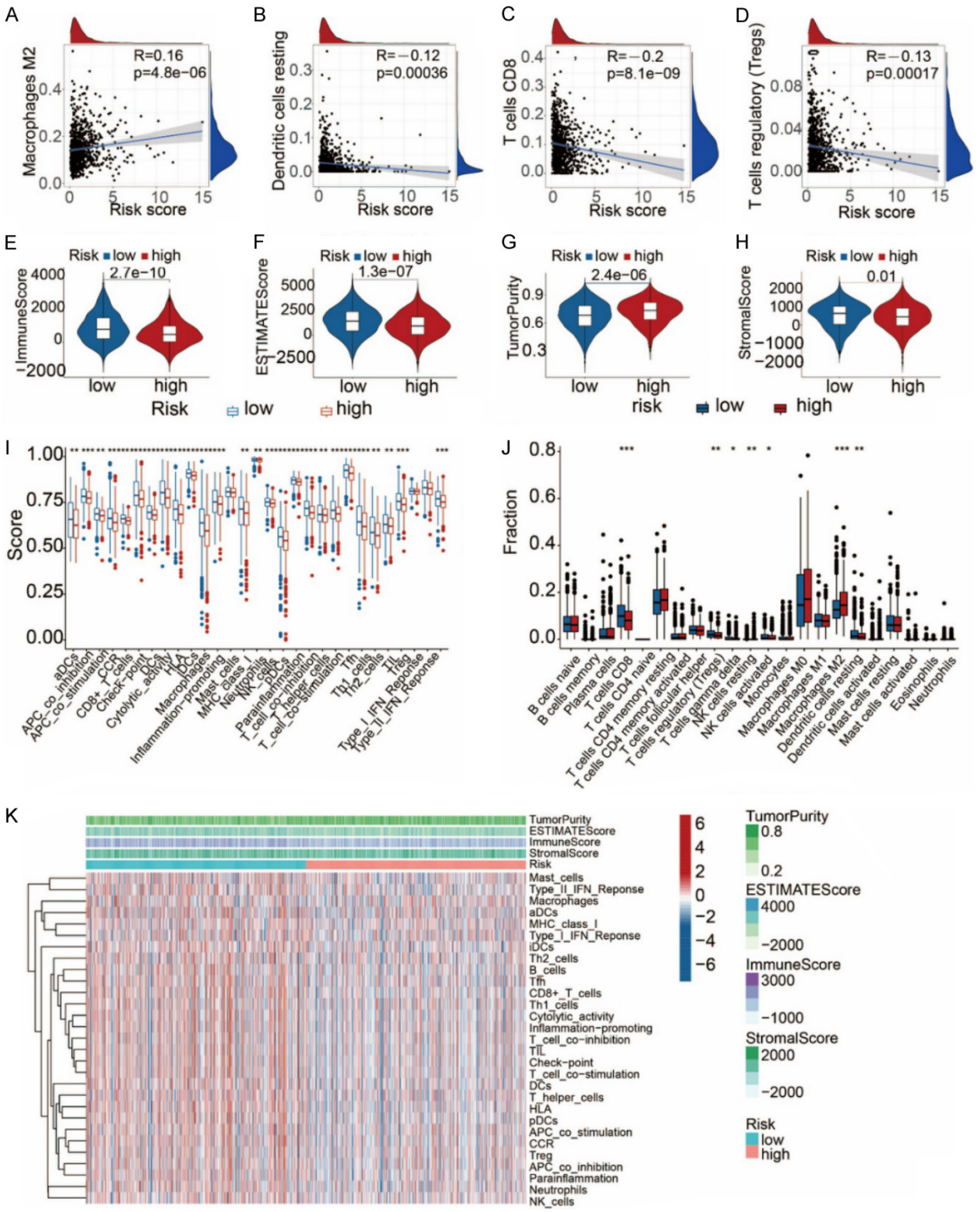

Figure 6. Correlation between infiltrating immune cells and ALL AS-based prognostic signature. (A) The relationship of risk score with M2 macrophages, (B) dendritic cells, (C) $CD8^+$ T cells, and (D) Tregs. The comparison of (E) immune score, (F) ESTIMATE score, (G) tumor purity, and (H) stromal score between the low- and high-risk groups. (I) The heatmap shows 29 immune signatures and scores in the two groups. Red indicates high expression, and blue indicates low expression. (J) Differences in the enrichment of immune-related signatures between the two groups. (K) The differences in infiltrating immune cell subsets and levels between the two risk groups.

further verification. First, we used TCGA data to analyze the differential expression of MAZ from multiple perspectives. Judging by the results, the expression of MAZ in tumor tissues is

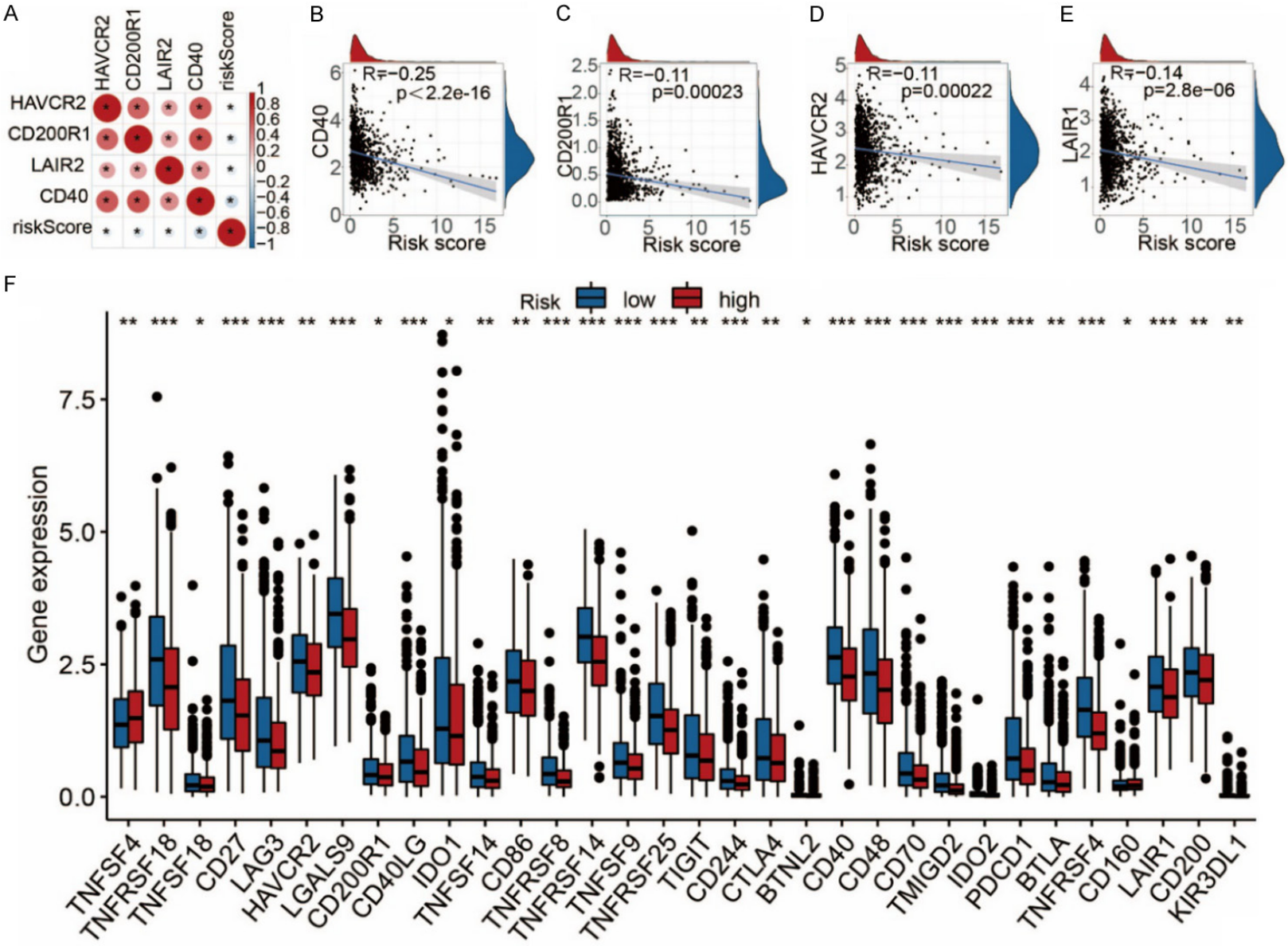

Figure 7. Association between ALL AS-based prognostic signature and immune checkpoint genes. (A) Association of immune checkpoint inhibitors *CD40, CD200R1, HAVCR2, and LAIR1* with risk score. (B) Correlation of risk score with CD40, (C) CD200R1, (D) HAVCR2, and (E) LAIR1. (F) The expression levels of genes related to immune checkpoint blockade.

noticeably higher than that in normal tissues (**Figure 8A**). Compared with early BC, MAZ was overexpressed in tumors in advanced BC (**Figure 8C** and **8D**). To estimate the prognostic value, we evaluated the survival of BC patients with high and low tumor expression of MAZ. The results indicate that the OS of patients with high expression of MAZ was significantly shorter than that of patients with low MAZ expression (**Figure 8B**). Furthermore, we found that the expression levels of 27 genes (such as *CD40* and *CD200R1*) were significantly different between subgroups (**Figure 8E**). Finally, the tumor purity was adjusted by TIMER, and the correlation between MAZ and immune checkpoint-related genes was assessed. The results of the TIMER analysis show that MAZ negatively correlated with CD40 (R = -0.135; P = 1.92e-05), CD200R1 (R = -0.187; P = 2.65e-09), HAVCR2 (R = -0.147; P = 3.22e-06), and LAIR1 (R = -0.105; P = 9.12e-04), suggesting that targeting MAZ may be useful for the treatment of BC via immune checkpoint blockade (**Figure 8F-J**).

Experimental verification of MAZ expression in BC

We carried out RT-qPCR to determine differences in MAZ expression in three BC cell lines (MDA-MB-231, MCF-7, and MDA-MB-468) versus normal human breast epithelial cells. MAZ was upregulated in BC, with the MCF-7 cell line having the highest expression (**Figure 9A**). To further verify MAZ expression in BC, western blotting was conducted to determine the levels of MAZ, and the results were consistent with those of RT-qPCR (**Figure 9B**). The immunofluorescence data revealed that BC tissues had stronger anti-MAZ staining than that of the adjacent normal tissues, thus confirming that MAZ is overexpressed in BC (**Figure 9C** and **9D**).

MAZ function in the tumor microenvironment

To further elucidate the relationship between MAZ and the tumor microenvironment, we analyzed MAZ from a number of different standpoints. First, BC patients were distributed into two groups based on the median MAZ expression level in the tumor. The stromal cell and immune cell infiltration scores of patients with high MAZ expression were found to be lower than those of patients with low MAZ expression. Therefore, the infiltration by stromal cells and immune cells in the samples with low MAZ expression seemed to be high, whereas BC patients with high MAZ expression in the tumor had higher tumor purity (**Figure 10A-D**). An arm-level gain is the main type of mutation in this context (**Figure 10E-I**). Here, the expression level of MAZ negatively correlated with $CD8^+$ T cells, macrophages, common lymphoid progenitors, and neutrophils (**Figure 10J-N**). The ssGSEA revealed that such indicators as antigen-presenting -cell co-inhibition, antigen-presenting -cell co-stimulation, B cells, chemokine receptors, immune checkpoint status, cytolytic activity, DCs, human leukocyte antigen, immature DCs, macrophages, neutrophils, NK cells, para-inflammation, T cell co-inhibition, all Th cells, Th2 cells, TILs, Tregs, a type I interferon response, and a type II interferon response decreased significantly with an increase in MAZ expression (**Figure 10O**). The results of CIBESORT analysis of the TCGA cohort revealed that patients with high levels of MAZ exhibited a significant increase in Treg numbers and M0 macrophages and a significant decrease in gamma delta T cell and DC activation (**Figure 10P**).

Construction of a model of the SF-AS regulatory network

To clarify the potential mechanism of AS, we used co-expression analysis to understand the relationships between SFs and AS, and we visualized the results as an SF-AS regulatory network. As illustrated in **Figure 11**, 23 upregulated AS events (red flags), 45 downregulated AS events (green ellipses), and 31 SFs (blue flags) were identified. In the proposed regulatory network, the co-expression coefficients of some SF-AS pairs were greater than 0.7. This finding suggests that these SFs may be an important part of the AS disorder of BC and are strongly related to the initiation and progression of such tumors.

Subgroup analysis of BCs of different molecular subtypes

To investigate whether the difference in expression is related to molecular subtypes of BC, subgroup analysis of BCs was performed. Patients were subdivided into subgroups HR(+), HER-2(+), and triple-negative BC (TNBC) based on receptor expression. As shown in Figure S10

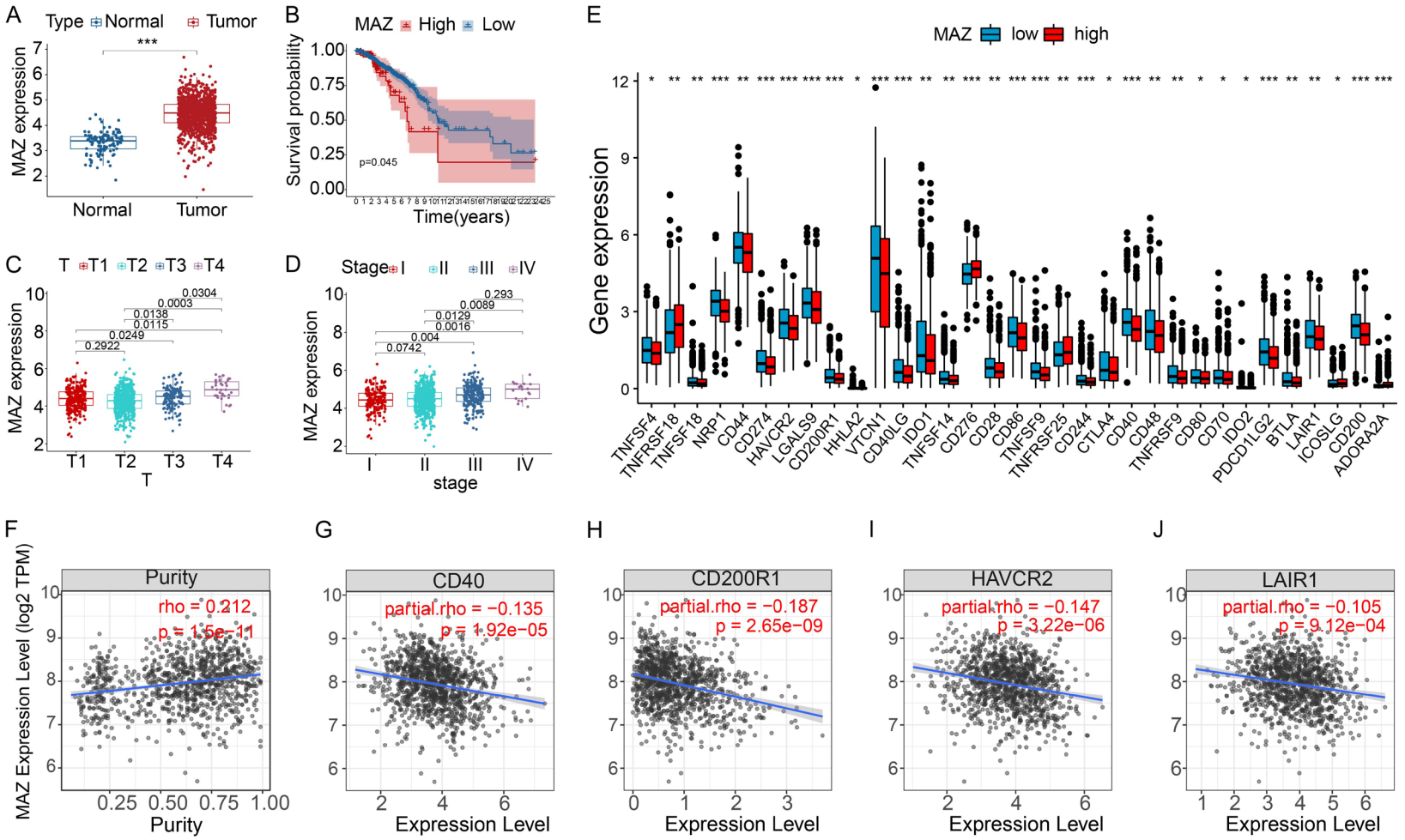

Figure 8. The clinical values of MAZ in BC and *in vitro*. (A) MAZ is overexpressed in BC tumor tissue. (B) Significant difference in MAZ expression between major pathological stages. (C) Association between risk score and tumor stage. (D) A lower MAZ level indicates longer overall survival. (E) The expression of genes related to immune checkpoint blockade. (F) Correlation between risk score and purity. Association of risk score with (G) *CD40*, (H) *CD200R1*, (I) *HAVCR2*, and (J) *LAIR1*.

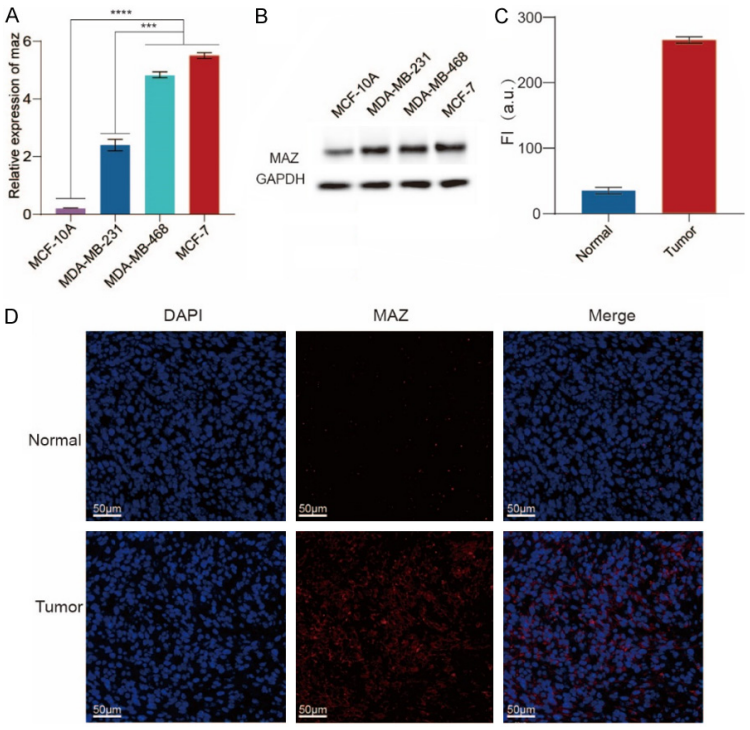

Figure 9. Validation of the biological functions of MAZ in BC and *in vivo*. A and B. MAZ is highly expressed in BC cells. C. MAZ shows stronger red fluorescence in BC than in adjacent tissues. D. Immunofluorescence illustrate the expression of MAZ in BC and adjacent tissues.

(panels A, B, D, E, and G), there was no obvious difference in the magnitude of immune features, risk scores, subsets and infiltration levels of immune cells, and prognosis among the three subgroups. We also found that compared with the Her-2(+) and HR(+) subgroups, patients in the TNBC subgroup had lower MAZ expression in the tumor, lower tumor purity, and a higher Estimate Score (Figure S10C and 10F-I).

Discussion

According to the most recent data, BC has the highest incidence of all cancers worldwide [2]. Although the mortality rate of BC patients has decreased by 40% since 1989, the effectiveness of BC treatments is still unsatisfactory owing to the high heterogeneity and complexity of BC pathogenesis [40, 41]. Immunotherapy has attracted the attention of most investigators as a new research hotspot in recent years in the field of oncology, although the application of immunotherapy in BC is still in its infancy [42, 43]. There is, therefore, a need to elucidate the function of the immune system in the initiation and progression of BC and to identify biomarkers that have strong prognostic ability.

AS is a process that regulates gene expression, and it underlies proteome diversity and complexity. Several important cellular processes are regulated by AS, such as proliferation, differentiation, development, and apoptosis [44, 45]. AS is also intimately involved in the initiation and progression of cancer, including BC [46, 47]. Differentially expressed genes have the potential to be good prognostic markers, and they may also represent good therapeutic targets. In contrast, the relationships between AS events, the tumor microenvironment, and immunotherapy efficacy remain unclear.

In this study, AS data were obtained in a systematic analysis of AS events in TCGA Splice Seq and BC samples. A total of 1,781 cases of AS events significantly related to survival were identified by univariate Cox regression analysis to assess the prognostic value of AS events. Next, a prognostic model of BC was created via comprehensive bioinformatics analysis. All eight prognostic signatures (AA, AP, AT, AD, ME, ES, RI, and ALL) compiled via the AS model manifested a strong ability to determine the prognosis of BC. To confirm the predictive ability of the prognostic model, Kaplan-Meier survival analysis, ROC curve analysis, and Cox regression analysis were performed, which all proved the strong predictive ability. When BC cases were grouped according to clinical parameters, this prognostic model still showed excellent prognostic performance: the higher the clinical stage and T stage, the higher the risk in the BC patients. Nonetheless, there was not an obvious difference in the BC prognosis between sexes, and this result may be due to our small number of BC specimens from male patients. To improve the practical significance of the model, the prognostic characteristics and clinical stages of the line map were included in the evaluation, and the prediction results were highly consistent with the

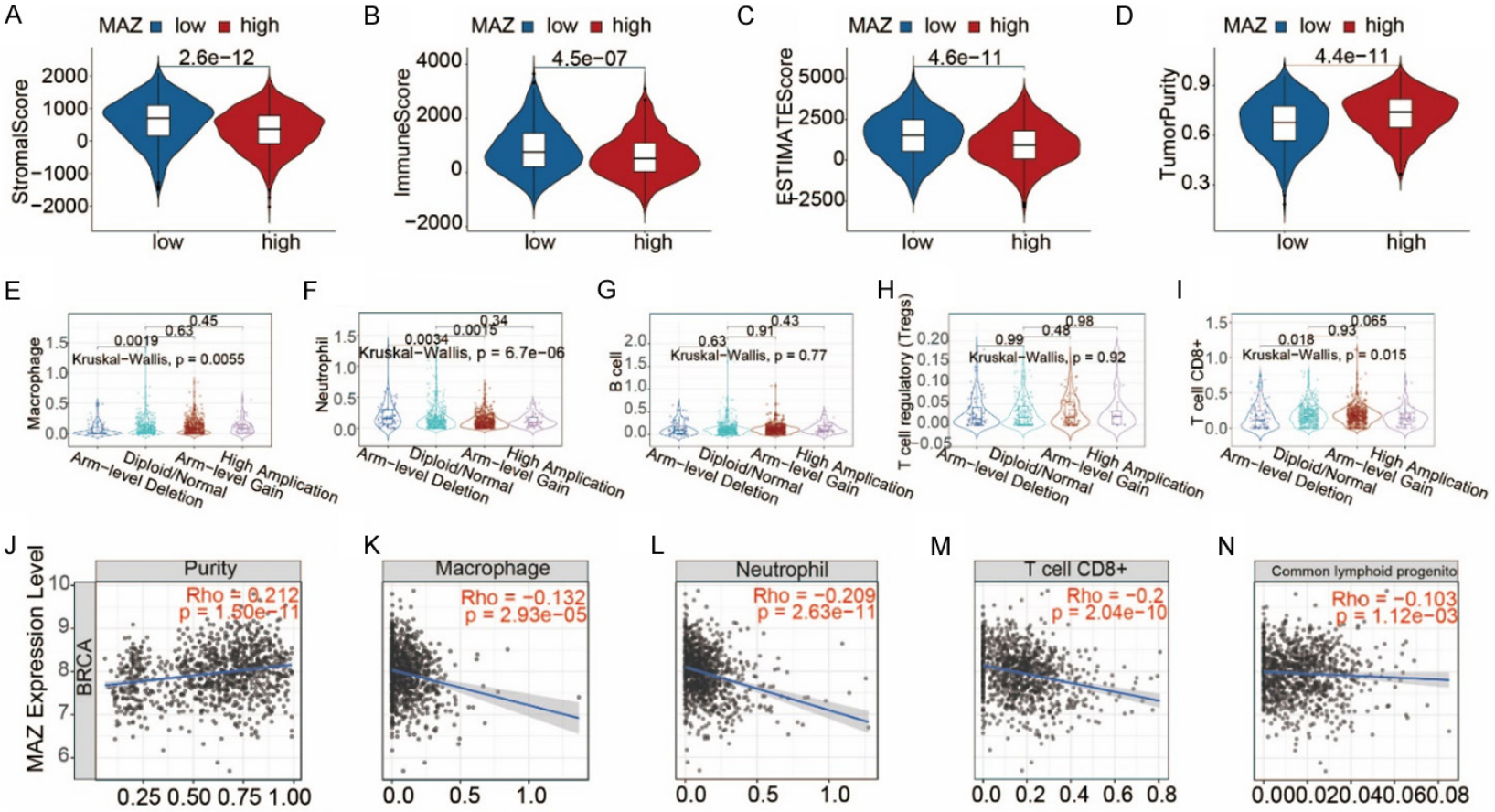
A
MAZ low high
2.6e-12
StromalScore
low high
B
MAZ low high
4.5e-07
ImmuneScore
low high
C
MAZ low high
4.6e-11
ESTIMATEScore
low high
D
MAZ low high
4.4e-11
TumorPurity
low high
E
Kruskal-Wallis, p = 0.0055
Macrophage
F
Kruskal-Wallis, p = 6.7e-06
Neutrophil
G
Kruskal-Wallis, p = 0.77
B cell
H
Kruskal-Wallis, p = 0.92
T cell regulatory (Tregs)
I
Kruskal-Wallis, p = 0.015
T cell CD8+
Arm-level Deletion
Diploid/Normal
Arm-level Gain
High Amplication
J
Purity
Rho = 0.212
p = 1.50e-11
MAZ Expression Level
BRCA
K
Macrophage
Rho = -0.132
p = 2.93e-05
L
Neutrophil
Rho = -0.209
p = 2.63e-11
M
T cell CD8+
Rho = -0.2
p = 2.04e-10
N
Common lymphoid progenito
Rho = -0.103
p = 1.12e-03

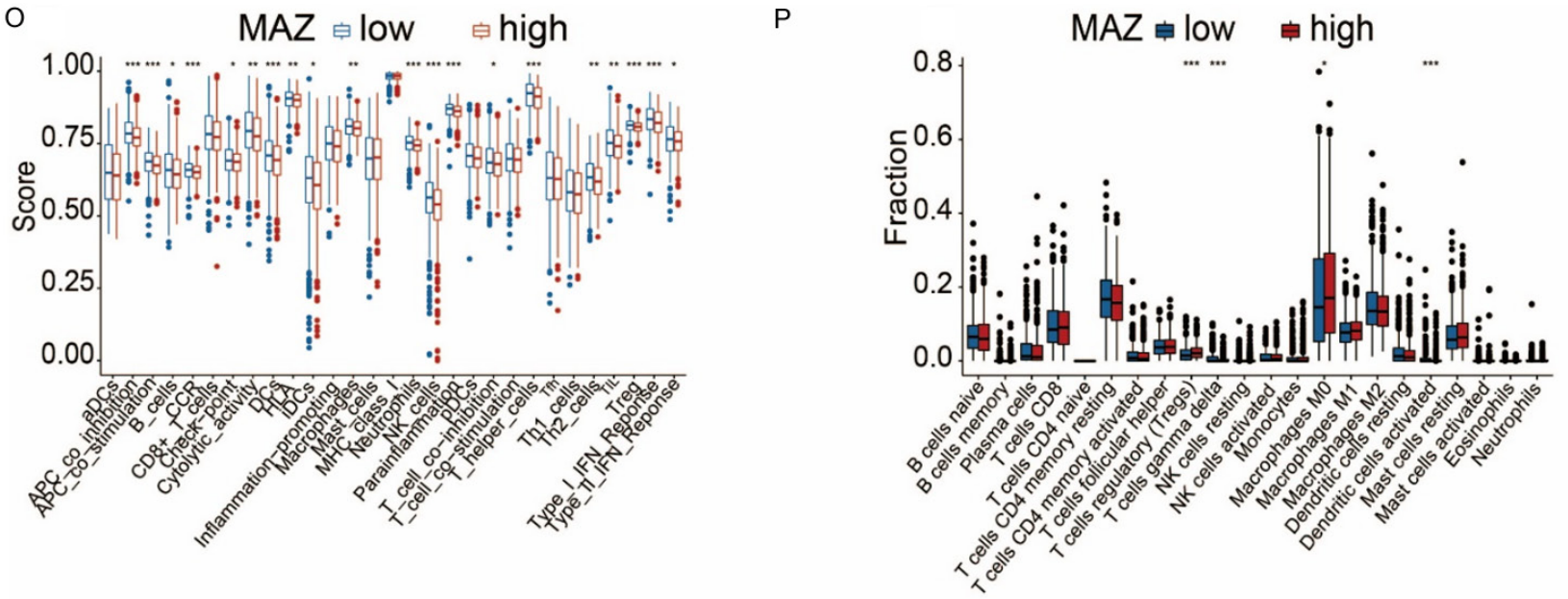

Figure 10. The role of MAZ in TIME features. A-D. The comparison of stromal, ESTIMATE, and immune scores and tumor purity between low and high MAZ expression groups. E-I. The copy number of immune cells in BC. J-N. The relationship of MAZ expression level with macrophage, neutrophil, $CD8^+$, and common lymphoid progenitor cells. O. The comparison of ssGSEA enrichment between low and high MAZ expression groups. P. The comparison of CIBERSORT results between low and high MAZ expression groups.

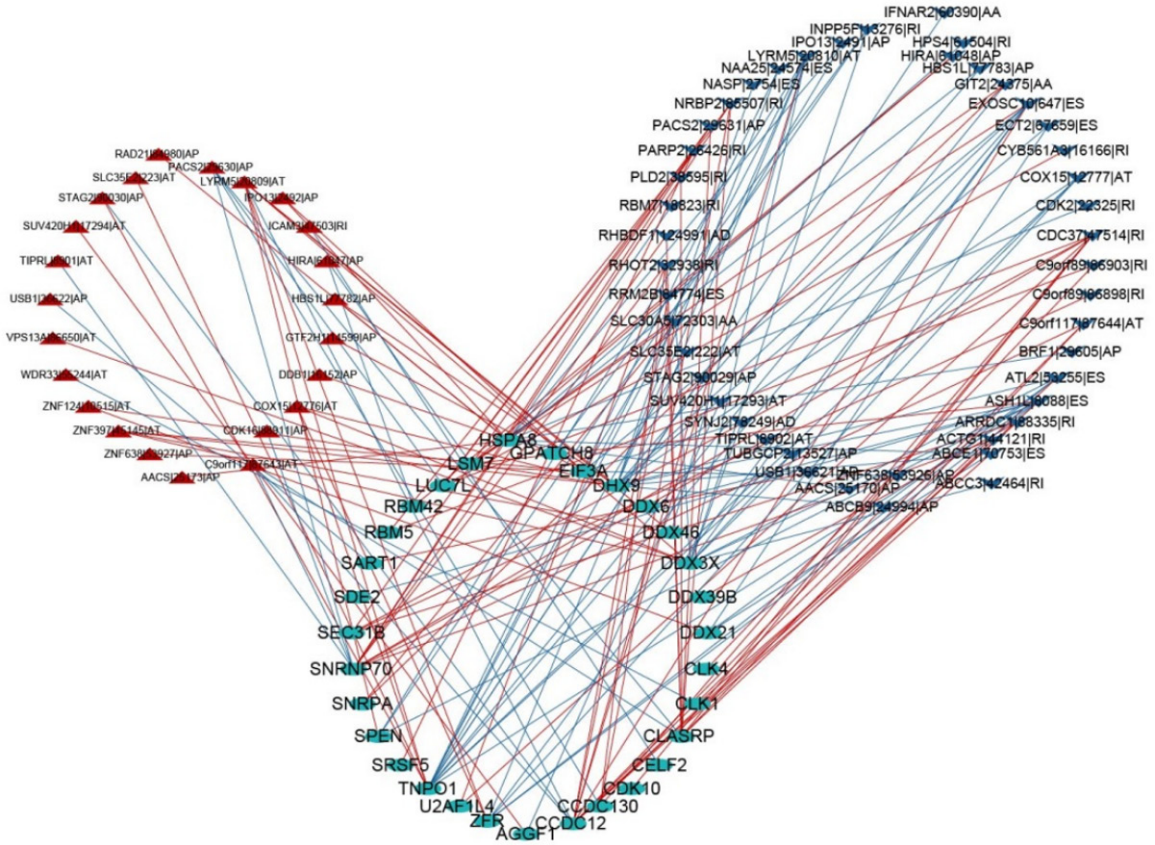

Figure 11. Construction of regulatory network of SFs and survival-related AS events. The red and blue arrows indicate a positive and negative correlation, respectively, between AS events and survival. Green ellipse represents SFs. The positive (r > 0.6) and negative (r < -0.6) correlations between SFs and AS events are shown in red and blue lines, respectively.

actual data. Furthermore, we constructed a regulatory network model from the most important inter-related SFs and AS modes in the TCGA-BRCA cohort.

To explore the relationship between AS events and the tumor immune microenvironment, we carried out TIMER, ESTIMATE, ssGSEA, and CIBERSORT analyses. The results indicate that infiltration by most immune cells negatively correlated with the risk in question, and the risk increased concurrently with tumor purity. These data mean that low immune cell infiltration is an indicator of poor prognosis. TILs were included in the 2019 WHO BC classification: the higher the degree of invasion by TILs, the better is the prognosis [48]. This principle is consistent with our finding that patients with a high risk had low TIL counts in the tumor. The risk score significantly negatively correlated with the expression levels of the four immune checkpoint-associated genes (*CD40*, *CD200R1*, *HAVCR2*, and *LAIR1*) that are strongly related to BC and with the expression levels of 33 immune checkpoint blockade-related genes (e.g., *PDCD1LG2*). These data suggest that the risk score could help formulate customized immunotherapy strategies and explain the poor effectiveness of immunotherapy in patients with advanced BC from another standpoint.

MAZ is a transcription factor that performs a dual regulatory function in the initiation and termination of target gene transcription [49-51]. To date, MAZ has been found at abnormally high levels in many types of tumors and is thought to affect the initiation and progression of tumors through a variety of signaling pathways. Yang et al. have reported that MAZ plays an important role in the pathogenesis of prostate cancer [52]. Triner et al. have found that MAZ overexpression can promote inflammatory progression of colon cancer [53]. Little is known, however, about the role of MAZ in BC. In

this study, TCGA data showed that MAZ was highly expressed in BC tumors, and the results suggest that such BC cases had a poor prognosis. MAZ expression positively correlated with the clinical stage and tumor grade. Moreover, a significant negative correlation was noted between MAZ expression and the immune checkpoint-related genes (*CD40*, *CD200R1*, *HAVCR2*, and *LAIR1*) associated with BC. The link between the genes related to immune checkpoints and the prognosis of BC remains unclear. According to the above analysis, there appears to be a connection between a low level of immune checkpoint-related gene expression and poor prognosis. Furthermore, patients with high expression of MAZ in the tumor had a relatively low degree of immune cell infiltration and stromal cell infiltration in the tumor and relatively low TIL numbers. These data provide further support for the correlation between poor prognosis and high MAZ levels.

To investigate the relevant cellular functions of MAZ, we conducted verification experiments. RT-qPCR revealed that MAZ expression was much higher in BC cell lines than that in corresponding normal cells. The MCF-7 cell line had the highest expression of MAZ. The western blotting results were highly consistent with the above RT-qPCR findings. To explore the function of MAZ in the initiation and progression of BC, we used an immunofluorescence assay to track the expression of MAZ. This showed that MAZ was overexpressed in BC, and its main expression site was the nucleus.

BC patients were subdivided into HR(+), Her-2(+), and TNBC subgroups according to the expression of relevant receptors [HR(+) means that human epidermal growth factor receptor 2 (Her-2) is absent, and one of estrogen receptor (ER) and progesterone receptor (PR) is present; HER-2(+) means that Her-2 is present; TNBC means that ER, PR, and HER-2 are absent]. The differences in the tumor immune microenvironment, risk score, *MAZ* expression, immune checkpoint gene expression, and survival probability among these subgroups were tested. The results show that compared with the Her-2(+) and HR(+) subgroups, patients in the TNBC subgroup had lower MAZ expression in the tumor, lower tumor purity, and a higher Estimate Score. This result is consistent with the data in the literature [54, 55] and our previous findings (**Figures 6**-**8**). It is well known that TNBC is associated with high immune cell infiltration and low tumor purity. Our preliminary results suggest that MAZ expression is negatively related to the level of immune cell infiltration (macrophages, neutrophils, $CD8^+$ T cells, and common lymphoid progenitors). These data further confirm that MAZ expression is significantly negatively correlated with tumor infiltration by immune cells.

Overall, patients with higher risk scores or higher tumor MAZ expression levels had lower immune cell abundances in the tumor, higher tumor purity, and shorter survival. Thus, it can be assumed that the antitumor effect of immune cells may be related to the blockade of immune checkpoint pathways. This is because the risk score and the level of MAZ are correlated with the expression of immune checkpoint suppressors.

Compared with previous studies on the creation of prognostic models for BC, the present study has some clear advantages.

1. We explored the relationship between AS and the tumor microenvironment and immunotherapy in BC.

2. The Estimate R Package, CiberSort method, ssGSEA algorithm, and TIMER database were employed to reveal the full picture of the tumor immune microenvironment in BC.

3. By a combination of TCGA data and our experiments, the likely function of MAZ in BC was identified.

Conclusion

We used prognosis-related AS events to build a prognostic model and we analyzed the model from three perspectives: clinical parameters, the tumor microenvironment, and differentially expressed genes. The prognostic model manifested a strong prognostic ability. Thus, in addition to devising a highly effective and robust nomogram to quantitatively evaluate BC prognosis, we also constructed a model of the AS-SF network, which may help visualize the proposed therapeutic targets in BC. A systematic bioinformatics analysis indicated a robust correlation of the BC tumor immune microenvironment with immunotherapy effectiveness, revealing that there may be a connection between poor prognosis and poor outcomes of

immunotherapy with low immune cell infiltration in BC. Finally, we identified MAZ as a highly differentially expressed gene, and bioinformatics analysis and experimental validation were performed to confirm that MAZ is strongly associated with BC prognosis.

Acknowledgements

We would like to thank Ethna for her unwavering support of this study, and we also would like to thank Editage (www.editage.cn) for English language editing. Supported by: Youth Fund Project of Guizhou Provincial People's Hospital [GZSYQN (2021) 14].

Disclosure of conflict of interest

None.

Address correspondence to: Dr. Qinglong Yang, Department of General Surgery, Guizhou Provincial People's Hospital, Guizhou 550000, Guiyang, China. Tel: +86-18569592010; E-mail: 715581746@qq.com

References

[1] Sung H, Ferlay J, Siegel RL, Laversanne M, Soerjomataram I, Jemal A and Bray F. Global cancer statistics 2020: GLOBOCAN estimates of incidence and mortality worldwide for 36 cancers in 185 countries. CA Cancer J Clin 2021; 71: 209-249.

[2] Siegel RL, Miller KD, Fuchs HE and Jemal A. Cancer statistics, 2021. CA Cancer J Clin 2021; 71: 7-33.

[3] Khaled N and Bidet Y. New insights into the implication of epigenetic alterations in the EMT of triple negative breast cancer. Cancers (Basel) 2019; 11: 559.

[4] Nicolini A, Ferrari P and Duffy MJ. Prognostic and predictive biomarkers in breast cancer: past, present and future. Semin Cancer Biol 2018; 52: 56-73.

[5] Bagaria SP, Ray PS, Sim MS, Ye X, Shamonki JM, Cui X and Giuliano AE. Personalizing breast cancer staging by the inclusion of ER, PR, and HER2. JAMA Surg 2014; 149: 125-129.

[6] Kim BK, Oh SJ, Song JY, Lee HB, Park MH, Jung Y, Park WC, Lee J and Sun WY; Korean Breast Cancer Society. Clinical characteristics and prognosis associated with multiple primary cancers in breast cancer patients. J Breast Cancer 2018; 21: 62-69.

[7] Lee J, Park S, Kim S, Kim J, Ryu J, Park HS, Kim SI and Park BW. Characteristics and survival of breast cancer patients with multiple synchronous or metachronous primary cancers. Yonsei Med J 2015; 56: 1213-1220.

[8] Yeo SK and Guan JL. Breast cancer: multiple subtypes within a tumor? Trends Cancer 2017; 3: 753-760.

[9] Frontiers Production Office. Erratum: immune tumor microenvironment in breast cancer and the participation of estrogen and its receptors in cancer physiopathology. Front Immunol 2019; 10: 1868.

[10] Yu T and Di G. Role of tumor microenvironment in triple-negative breast cancer and its prognostic significance. Chin J Cancer Res 2017; 29: 237-252.

[11] Xu N, Palmer DC, Robeson AC, Shou P, Bommiasamy H, Laurie SJ, Willis C, Dotti G, Vincent BG, Restifo NP and Serody JS. STING agonist promotes CAR T cell trafficking and persistence in breast cancer. J Exp Med 2021; 218: e20200844.

[12] Hu ZI and McArthur HL. Immunotherapy in breast cancer: the new frontier. Curr Breast Cancer Rep 2018; 10: 35-40.

[13] Yu LY, Tang J, Zhang CM, Zeng WJ, Yan H, Li MP and Chen XP. New immunotherapy strategies in breast cancer. Int J Environ Res Public Health 2017; 14: 68.

[14] Cha JH, Yang WH, Xia W, Wei Y, Chan LC, Lim SO, Li CW, Kim T, Chang SS, Lee HH, Hsu JL, Wang HL, Kuo CW, Chang WC, Hadad S, Purdie CA, McCoy AM, Cai S, Tu Y, Litton JK, Mittendorf EA, Moulder SL, Symmans WF, Thompson AM, Piwnica-Worms H, Chen CH, Khoo KH and Hung MC. Metformin promotes antitumor immunity via endoplasmic-reticulum-associated degradation of PD-L1. Mol Cell 2018; 71: 606-620.

[15] Basu A, Ramamoorthi G, Jia Y, Faughn J, Wiener D, Awshah S, Kodumudi K and Czerniecki BJ. Immunotherapy in breast cancer: current status and future directions. Adv Cancer Res 2019; 143: 295-349.

[16] de Melo Gagliato D, Buzaid AC, Perez-Garcia J and Cortes J. Immunotherapy in breast cancer: current practice and clinical challenges. BioDrugs 2020; 34: 611-623.

[17] Esteva FJ, Hubbard-Lucey VM, Tang J and Pusztai L. Immunotherapy and targeted therapy combinations in metastatic breast cancer. Lancet Oncol 2019; 20: e175-e186.

[18] Keenan TE and Tolaney SM. Role of immunotherapy in triple-negative breast cancer. J Natl Compr Canc Netw 2020; 18: 479-489.

[19] Bartsch R and Bergen E. SABCS 2017: update on chemotherapy, targeted therapy, and immunotherapy. Memo 2018; 11: 204-207.

[20] Williams AD, Payne KK, Posey AD Jr, Hill C, Conejo-Garcia J, June CH and Tchou J. Immunotherapy for breast cancer: current and fu-

ture strategies. Curr Surg Rep 2017; 5: 1245-1261.
[21] Climente-González H, Porta-Pardo E, Godzik A and Eyras E. The functional impact of alternative splicing in cancer. Cell Rep 2017; 20: 2215-2226.
[22] Baralle FE and Giudice J. Alternative splicing as a regulator of development and tissue identity. Nat Rev Mol Cell Biol 2017; 18: 437-451.
[23] Ule J and Blencowe BJ. Alternative splicing regulatory networks: functions, mechanisms, and evolution. Mol Cell 2019; 76: 329-345.
[24] Zhao S. Alternative splicing, RNA-seq and drug discovery. Drug Discov Today 2019; 24: 1258-1267.
[25] Demircioglu D, Cukuroglu E, Kindermans M, Nandi T, Calabrese C, Fonseca NA, Kahles A, Lehmann KV, Stegle O, Brazma A, Brooks AN, Ratsch G, Tan P and Goke J. A pan-cancer transcriptome analysis reveals pervasive regulation through alternative promoters. Cell 2019; 178: 1465-1477.
[26] Ouyang JW, Zhang YJ, Xiong F, Zhang SS, Gong ZJ, Yan QJ, He Y, Wei F, Zhang WL, Zhou M, Xiang B, Wang FY, Li XL, Li Y, Li GY, Zeng ZY, Guo C and Xiong W. The role of alternative splicing in human cancer progression. Am J Cancer Res 2021; 11: 4642-4667.
[27] Pradella D, Naro C, Sette C and Ghigna C. EMT and stemness: flexible processes tuned by alternative splicing in development and cancer progression. Mol Cancer 2017; 16: 8.
[28] Ni M, Zhou X, Liu J, Yu H, Gao Y, Zhang X and Li Z. Prediction of the clinicopathological subtypes of breast cancer using a fisher discriminant analysis model based on radiomic features of diffusion-weighted MRI. BMC Cancer 2020; 20: 1073.
[29] Venables JP, Klinck R, Bramard A, Inkel L, Dufresne-Martin G, Koh C, Gervais-Bird J, Lapointe E, Froehlich U, Durand M, Gendron D, Brosseau JP, Thibault P, Lucier JF, Tremblay K, Prinos P, Wellinger RJ, Chabot B, Rancourt C and Elela SA. Identification of alternative splicing markers for breast cancer. Cancer Res 2008; 68: 9525-9531.
[30] Blanche P, Dartigues JF and Jacqmin-Gadda H. Estimating and comparing time-dependent areas under receiver operating characteristic curves for censored event times with competing risks. Stat Med 2013; 32: 5381-5397.
[31] Darvin P, Toor SM, Sasidharan Nair V and Elkord E. Immune checkpoint inhibitors: recent progress and potential biomarkers. Exp Mol Med 2018; 50: 1-11.
[32] Ma HS, Poudel B, Torres ER, Sidhom JW, Robinson TM, Christmas B, Scott B, Cruz K, Woolman S, Wall VZ, Armstrong T and Jaffee EM. A CD40 agonist and PD-1 antagonist antibody reprogram the microenvironment of nonimmunogenic tumors to allow T-cell-mediated anticancer activity. Cancer Immunol Res 2019; 7: 428-442.
[33] Erin N, Dilmaç S, Curry A, Duymuş Ö, Tanriover G, Prodeus A, Gariepy J and Gorczynski RM. CD200 mimetic aptamer PEG-M49 markedly increases the therapeutic effects of pegylated liposomal doxorubicin in a mouse model of metastatic breast carcinoma: an effect independent of CD200 receptor 1. Cancer Immunol Immunother 2020; 69: 103-114.
[34] Corti C, Nicolò E and Curigliano G. Novel immune targets for the treatment of triple-negative breast cancer. Expert Opin Ther Targets 2021; 25: 815-834.
[35] Miao X, Guo Q, Pan Z, Xu X, Shao X and Wang X. The characteristics and novel clinical implications of CD4+CXCR5+Foxp3+ follicular regulatory T cells in breast cancer. Ann Transl Med 2021; 9: 1332.
[36] Joseph C, Alsaleem MA, Toss MS, Kariri YA, Althobiti M, Alsaeed S, Aljohani AI, Narasimha PL, Mongan NP, Green AR and Rakha EA. The ITIM-containing receptor: leukocyte-associated immunoglobulin-like receptor-1 (LAIR-1) modulates immune response and confers poor prognosis in invasive breast carcinoma. Cancers (Basel) 2020; 13: 80.
[37] Seiler M, Peng S, Agrawal AA, Palacino J, Teng T, Zhu P, Smith PG, Buonamici S and Yu L. Somatic mutational landscape of splicing factor genes and their functional consequences across 33 cancer types. Cell reports 2018; 23: 282-296.
[38] Binnewies M, Roberts EW, Kersten K, Chan V, Fearon DF, Merad M, Coussens LM, Gabrilovich DI, Ostrand-Rosenberg S, Hedrick CC, Vonderheide RH, Pittet MJ, Jain RK, Zou W, Howcroft TK, Woodhouse EC, Weinberg RA and Krummel MF. Understanding the tumor immune microenvironment (TIME) for effective therapy. Nat Med 2018; 24: 541-550.
[39] Gonzalez H, Hagerling C and Werb Z. Roles of the immune system in cancer: from tumor initiation to metastatic progression. Genes Dev 2018; 32: 1267-1284.
[40] DeSantis CE, Ma J, Gaudet MM, Newman LA, Miller KD, Goding Sauer A, Jemal A and Siegel RL. Breast cancer statistics, 2019. CA Cancer J Clin 2019; 69: 438-451.
[41] Pedrosa RMSM, Mustafa DA, Soffietti R and Kros JM. Breast cancer brain metastasis: molecular mechanisms and directions for treatment. Neuro Oncol 2018; 20: 1439-1449.
[42] Emens LA. Breast cancer immunotherapy: facts and hopes. Clin Cancer Res 2018; 24: 511-520.

[43] Hegde PS and Chen DS. Top 10 challenges in cancer immunotherapy. Immunity 2020; 52: 17-35.
[44] Bates DO, Morris JC, Oltean S and Donaldson LF. Pharmacology of modulators of alternative splicing. Pharmacol Rev 2017; 69: 63-79.
[45] Simms BA and Zamponi GW. Neuronal voltage-gated calcium channels: structure, function, and dysfunction. Neuron 2014; 82: 24-45.
[46] Montes M, Sanford BL, Comiskey DF and Chandler DS. RNA splicing and disease: animal models to therapies. Trends Genet 2019; 35: 68-87.
[47] Sciarrillo R, Wojtuszkiewicz A, Assaraf YG, Jansen G, Kaspers GJL, Giovannetti E and Cloos J. The role of alternative splicing in cancer: from oncogenesis to drug resistance. Drug Resist Updat 2020; 53: 100728.
[48] Denkert C, von Minckwitz G, Darb-Esfahani S, Lederer B, Heppner BI, Weber KE, Budczies J, Huober J, Klauschen F, Furlanetto J, Schmitt WD, Blohmer JU, Karn T, Pfitzner BM, Kümmel S, Engels K, Schneeweiss A, Hartmann A, Noske A, Fasching PA, Jackisch C, van Mackelenbergh M, Sinn P, Schem C, Hanusch C, Untch M and Loibl S. Tumour-infiltrating lymphocytes and prognosis in different subtypes of breast cancer: a pooled analysis of 3771 patients treated with neoadjuvant therapy. Lancet Oncol 2018; 19: 40-50.
[49] Li H, Yang F, Hu A, Wang X, Fang E, Chen Y, Li D, Song H, Wang J, Guo Y, Liu Y, Li H, Huang K, Zheng L and Tong Q. Therapeutic targeting of circ-CUX1/EWSR1/MAZ axis inhibits glycolysis and neuroblastoma progression. EMBO Mol Med 2019; 11: e10835.
[50] Gao P, Chen C, Howell ED, Li Y, Tober J, Uzun Y, He B, Gao L, Zhu Q, Siekmann AF, Speck NA and Tan K. Transcriptional regulatory network controlling the ontogeny of hematopoietic stem cells. Genes Dev 2020; 34: 950-964.
[51] Maity G, Haque I, Ghosh A, Dhar G, Gupta V, Sarkar S, Azeem I, McGregor D, Choudhary A, Campbell DR, Kambhampati S, Banerjee SK and Banerjee S. The MAZ transcription factor is a downstream target of the oncoprotein Cyr61/CCN1 and promotes pancreatic cancer cell invasion via CRAF-ERK signaling. J Biol Chem 2018; 293: 4334-4349.
[52] Yang Q, Lang C, Wu Z, Dai Y, He S, Guo W, Huang S, Du H, Ren D and Peng X. MAZ promotes prostate cancer bone metastasis through transcriptionally activating the KRas-dependent RalGEFs pathway. J Exp Clin Cancer Res 2019; 38: 391.
[53] Triner D, Castillo C, Hakim JB, Xue X, Greenson JK, Nuñez G, Chen GY, Colacino JA and Shah YM. Myc-associated zinc finger protein regulates the proinflammatory response in colitis and colon cancer via STAT3 signaling. Mol Cell Biol 2018; 38: e00386-18.
[54] Naik A and Decock J. Lactate metabolism and immune modulation in breast cancer: a focused review on triple negative breast tumors. Front Oncol 2020; 10: 598626.
[55] Schmidt M and Heimes AS. Immunomodulating therapies in breast cancer-from prognosis to clinical practice. Cancers (Basel) 2021; 13: 4883.

Table S2. The list of splicing factors (SF) genes

Splicing factors (SF) genes									
ACIN1	CRNKL1	EIF2S2	HNRNPUL1	MBNL2	PRPF18	RBM7	SNRNP40	TFIP11	ZMYM3
AGGF1	CSN3	EIF3A	HNRNPUL2	MBNL3	PRPF19	RBM8A	SNRNP48	THOC1	ZNF131
ALYREF	CTNNBL1	EIF4A3	HSPA1A	MFAP1	PRPF3	RBMS1	SNRNP70	THOC2	ZNF207
AQR	CWC15	ELAVL1	HSPA1B	MFSD11	PRPF31	RBMX	SNRPA	THOC3	ZNF326
ARGLU1	CWC22	ELAVL2	HSPA5	MOV10	PRPF38A	RBMX2	SNRPA1	THOC5	ZNF346
BAG2	CWC25	ELAVL3	HSPA8	MSI1	PRPF38B	RBMXL1	SNRPB	THOC6	ZNF830
BCAS1	CWC27	ELAVL4	HSPB1	MSI2	PRPF39	RBMXL2	SNRPB2	THOC7	ZRSR1
BCAS2	CXorf56	FAM32A	HTATSF1	MYEF2	PRPF4	RNF113A	SNRPC	THRAP3	ZRSR2
BUB3	DDX1	FAM50A	IGF2BP3	NCBP1	PRPF40A	RNF20	SNRPD1	TIA1	
BUD13	DDX17	FAM50B	IK	NCBP2	PRPF40B	RNF213	SNRPD2	TIAL1	
BUD31	DDX18	FAM58A	ILF2	NELFE	PRPF4B	RNF34	SNRPD3	TNPO1	
C17orf85	DDX19A	FMR1	ILF3	NKAP	PRPF6	RNF40	SNRPE	TOE1	
C19orf43	DDX19B	FRA10AC1	INTS1	NONO	PRPF8	RNPC3	SNRPF	TOP1MT	
SDE2	DDX20	FRG1	INTS3	NOSIP	PSEN1	RNPS1	SNRPG	TOPORS	
C1QBP	DDX21	FUBP1	INTS4	NOVA1	PSIP1	RNU1-1	SNRPN	TRA2A	
C9orf78	DDX23	FUBP3	INTS5	NOVA2	PTBP1	RNU2-1	SNU13	TRA2B	
CACTIN	DDX26B	FUS	INTS6	NRIP2	PTBP2	RNU4-1	SNURF	TRIM24	
CCAR1	DDX27	GEMIN2	INTS7	NSRP1	PTBP3	RNU5A-1	SNW1	TTC14	
CCDC12	DDX39A	GEMIN5	ISY1	NUDT21	PUF60	RNU6-1	SPEN	TXNL4A	
CCDC130	DDX39B	GNB2L1	JUP	NUMA1	QKI	SAP18	SREK1	U2AF1	
CCDC75	DDX3X	GPATCH1	KHDRBS1	PABPC1	RALY	SAP30BP	SRPK1	U2AF1L4	
CCDC94	DDX3Y	GPATCH3	KHDRBS3	PAXBP1	RALYL	SART1	SRPK2	U2AF2	
CD2BP2	DDX41	GPATCH8	KHSRP	PCBP1	RAVER1	SEC31B	SRPK3	U2SURP	
CDC40	DDX42	GPKOW	KIAA1429	PCBP2	RAVER2	SF1	SRRM1	UBL5	
CDC5L	DDX46	GRSF1	KIAA1967	PCBP3	RBBP6	SF3A1	SRRM2	USP39	
CDK10	DDX5	HNRNPA0	KIN	PCBP4	RBFOX2	SF3A2	SRRT	WBP11	
CDK11A	DDX50	HNRNPA1	LENG1	PDCD7	RBM10	SF3A3	SRSF1	WBP4	
CDK12	DDX6	HNRNPA2B1	LOC649330	PHF5A	RBM14	SF3B1	SRSF10	WDR77	
CELF1	DGCR14	HNRNPA3	LSM1	PLRG1	RBM15	SF3B2	SRSF11	WDR83	
CELF2	DHX15	HNRNPAB	LSM10	PNN	RBM15B	SF3B3	SRSF12	WTAP	
CELF3	DHX16	HNRNPC	LSM2	PPIE	RBM17	SF3B4	SRSF2	XAB2	
CELF4	DHX30	HNRNPCL1	LSM3	PPIG	RBM22	SF3B5	SRSF3	YBX1	
CELF5	DHX34	HNRNPD	LSM4	PPIH	RBM23	SF3B6	SRSF4	YBX3	
CELF6	DHX35	HNRNPDL	LSM5	PPIL1	RBM25	SFPQ	SRSF5	ZC3H11A	
CFAP20	DHX36	HNRNPF	LSM6	PPIL2	RBM26	SKIV2L2	SRSF6	ZC3H13	
CHERP	DHX38	HNRNPH1	LSM7	PPIL3	RBM27	SLU7	SRSF7	ZC3H18	
CIRBP	DHX40	HNRNPH2	LSM8	PPIL4	RBM3	SMN1	SRSF8	ZC3H4	
CLASRP	DHX57	HNRNPH3	LSMD1	PPM1G	RBM39	SMNDC1	SRSF9	ZC3HAV1	
CLK1	DHX8	HNRNPK	LUC7L	PPP1CA	RBM4	SMU1	SSB	ZCCHC10	
CLK2	DHX9	HNRNPL	LUC7L2	PPP1R8	RBM42	SNIP1	SUGP1	ZCCHC8	
CLK3	DNAJC6	HNRNPLL	LUC7L3	PPWD1	RBM45	SNRNP200	SYF2	ZCRB1	
CLK4	DNAJC8	HNRNPM	MAGOH	PQBP1	RBM47	SNRNP25	SYNCRIP	ZFR	
CLNS1A	EEF1A1	HNRNPR	MATR3	PRCC	RBM4B	SNRNP27	TAF15	ZMAT2	
CPSF6	EFTUD2	HNRNPU	MBNL1	PRMT5	RBM5	SNRNP35	TCERG1	ZMAT5	

Table S3. Results of correlation between alternative splicing events and splicing factors

Splicing factor	Alternative splicing	Correlation	*P*-value	Regulation
RBM42	HIRA|61048|AP	0.639363	7.82E-125	positive
RBM42	HIRA|61047|AP	-0.63365	5.62E-122	negative
CLASRP	RHOT2|32938|RI	0.702129	9.72E-161	positive
CLASRP	ACTG1|44121|RI	0.622965	8.66E-117	positive
CLASRP	C9orf117|87644|AT	0.634014	3.72E-122	positive
CLASRP	RHBDF1|124991|AD	0.617747	2.50E-114	positive
CLASRP	NRBP2|85507|RI	0.674913	4.49E-144	positive
CLASRP	C9orf117|87643|AT	-0.62744	6.18E-119	negative
CLASRP	PACS2|29630|AP	-0.64975	3.44E-130	negative
CLASRP	CDC37|47514|RI	0.697608	7.69E-158	positive
CLASRP	PLD2|38595|RI	0.604528	2.68E-108	positive
CLASRP	PACS2|29631|AP	0.603141	1.11E-107	positive
DDX46	LYRM5|20810|AT	-0.60997	9.56E-111	negative
DDX46	LYRM5|20809|AT	0.609968	9.56E-111	positive
DDX46	ZNF397|45145|AT	0.633061	1.10E-121	positive
SEC31B	C9orf89|86898|RI	0.604825	1.97E-108	positive
SEC31B	PARP2|26426|RI	0.654994	5.68E-133	positive
SEC31B	CDC37|47514|RI	0.654018	1.89E-132	positive
SEC31B	ARRDC1|88335|RI	0.668708	1.60E-140	positive
DDX6	ASH1L|8088|ES	-0.60458	2.53E-108	negative
HSPA8	HPS4|61504|RI	-0.61638	1.08E-113	negative
HSPA8	ABCE1|70753|ES	-0.63138	7.42E-121	negative
HSPA8	HBS1L|77783|AP	-0.60486	1.90E-108	negative
HSPA8	HBS1L|77782|AP	0.604862	1.90E-108	positive
HSPA8	AACS|25173|AP	0.6102	7.50E-111	positive
HSPA8	BRF1|29605|AP	-0.60112	8.64E-107	negative
HSPA8	AACS|25170|AP	-0.60108	9.04E-107	negative
HSPA8	RBM7|18823|RI	-0.60813	6.48E-110	negative
HSPA8	CDK2|22325|RI	-0.60022	2.15E-106	negative
HSPA8	DDB1|16152|AP	0.649116	7.44E-130	positive
HSPA8	IPO13|2491|AP	-0.60423	3.62E-108	negative
HSPA8	IPO13|2492|AP	0.604236	3.61E-108	positive
HSPA8	RAD21|84980|AP	0.636807	1.51E-123	positive
TNPO1	TUBGCP2|13527|AP	-0.60675	2.72E-109	negative
TNPO1	SLC35E2|222|AT	-0.60995	9.76E-111	negative
TNPO1	SLC35E2|223|AT	0.609949	9.76E-111	positive
TNPO1	LYRM5|20810|AT	-0.66657	2.55E-139	negative
TNPO1	LYRM5|20809|AT	0.666572	2.55E-139	positive
TNPO1	STAG2|90030|AP	0.631654	5.44E-121	positive
TNPO1	GIT2|24375|AA	-0.60642	3.81E-109	negative
TNPO1	NAA25|24574|ES	-0.60133	6.98E-107	negative
TNPO1	EXOSC10|647|ES	-0.67837	4.33E-146	negative
TNPO1	COX15|12777|AT	-0.60717	1.76E-109	negative
TNPO1	COX15|12776|AT	0.607168	1.76E-109	positive
TNPO1	SLC30A5|72303|AA	-0.68912	1.52E-152	negative
TNPO1	IFNAR2|60390|AA	-0.60165	5.08E-107	negative
TNPO1	ASH1L|8088|ES	-0.7004	1.27E-159	negative

TNPO1	STAG2|90029|AP	-0.6287	1.50E-119	negative
CCDC130	RHOT2|32938|RI	0.680892	1.40E-147	positive
CCDC130	NRBP2|85507|RI	0.618662	9.33E-115	positive
CCDC130	PACS2|29630|AP	-0.6141	1.23E-112	negative
CCDC130	CDC37|47514|RI	0.682784	1.05E-148	positive
CLK1	WDR33|55244|AT	-0.62604	2.92E-118	negative
CLK1	ARRDC1|88335|RI	0.608651	3.78E-110	positive
LUC7L	CYB561A3|16166|RI	0.620171	1.82E-115	positive
LUC7L	NRBP2|85507|RI	0.616123	1.43E-113	positive
LUC7L	PACS2|29630|AP	-0.65545	3.24E-133	negative
LUC7L	CDC37|47514|RI	0.634174	3.10E-122	positive
LUC7L	PACS2|29631|AP	0.631385	7.36E-121	positive
U2AF1L4	RHOT2|32938|RI	0.649365	5.50E-130	positive
U2AF1L4	CDC37|47514|RI	0.664367	4.33E-138	positive
RBM5	PARP2|26426|RI	0.601422	6.37E-107	positive
RBM5	C9orf89|86903|RI	0.674901	4.56E-144	positive
CELF2	ICAM3|47503|RI	-0.60769	1.03E-109	negative
CDK10	CDC37|47514|RI	0.625239	7.09E-118	positive
SRSF5	PARP2|26426|RI	0.613808	1.68E-112	positive
LSM7	HIRA|61048|AP	0.603797	5.67E-108	positive
LSM7	HIRA|61047|AP	-0.60307	1.19E-107	negative
LSM7	GIT2|24375|AA	0.625389	6.00E-118	positive
LSM7	EXOSC10|647|ES	0.628235	2.54E-119	positive
LSM7	SLC30A5|72303|AA	0.662215	6.73E-137	positive
LSM7	ASH1L|8088|ES	0.630215	2.76E-120	positive
DDX21	ZNF124|10515|AT	0.608772	3.33E-110	positive
DDX21	ABCE1|70753|ES	-0.63608	3.49E-123	negative
DDX21	ATL2|53255|ES	-0.601	9.74E-107	negative
DDX21	ECT2|67659|ES	-0.60887	3.02E-110	negative
EIF3A	ZNF638|53927|AP	0.604081	4.24E-108	positive
EIF3A	SYNJ2|78249|AD	-0.60256	2.00E-107	negative
EIF3A	ZNF638|53926|AP	-0.61149	1.93E-111	negative
EIF3A	GTF2H1|14599|AP	0.612682	5.52E-112	positive
EIF3A	EXOSC10|647|ES	-0.65307	6.08E-132	negative
EIF3A	IPO13|2491|AP	-0.60345	8.08E-108	negative
EIF3A	IPO13|2492|AP	0.603452	8.06E-108	positive
EIF3A	ZNF397|45145|AT	0.607672	1.05E-109	positive
SART1	USB1|36622|AP	-0.63691	1.35E-123	negative
SART1	USB1|36621|AP	0.645437	6.12E-128	positive
DDX39B	ARRDC1|88335|RI	0.645614	4.96E-128	positive
CCDC12	ABCE1|70753|ES	0.616855	6.51E-114	positive
CCDC12	C9orf117|87644|AT	0.613377	2.65E-112	positive
CCDC12	ABCB9|24994|AP	0.632084	3.34E-121	positive
CCDC12	C9orf117|87643|AT	-0.60805	7.07E-110	negative
CCDC12	LYRM5|20810|AT	0.633782	4.85E-122	positive
CCDC12	LYRM5|20809|AT	-0.63378	4.85E-122	negative
CCDC12	STAG2|90030|AP	-0.6303	2.49E-120	negative
CCDC12	RRM2B|84774|ES	0.604697	2.25E-108	positive
CCDC12	ATL2|53255|ES	0.608482	4.51E-110	positive

CCDC12	EXOSC10|647|ES	0.631658	5.41E-121	positive
CCDC12	SLC30A5|72303|AA	0.615493	2.79E-113	positive
CCDC12	ASH1L|8088|ES	0.656489	8.92E-134	positive
CCDC12	STAG2|90029|AP	0.619728	2.94E-115	positive
SDE2	ASH1L|8088|ES	-0.60086	1.13E-106	negative
DHX9	NASP|2754|ES	-0.62698	1.03E-118	negative
DHX9	ZNF124|10515|AT	0.618219	1.50E-114	positive
DHX9	ABCE1|70753|ES	-0.64171	5.00E-126	negative
DHX9	ABCB9|24994|AP	-0.60379	5.71E-108	negative
DHX9	HBS1L|77783|AP	-0.60236	2.46E-107	negative
DHX9	HBS1L|77782|AP	0.602359	2.46E-107	positive
DHX9	LYRM5|20810|AT	-0.63954	6.39E-125	negative
DHX9	LYRM5|20809|AT	0.639531	6.43E-125	positive
DHX9	NAA25|24574|ES	-0.60354	7.40E-108	negative
DHX9	ATL2|53255|ES	-0.64954	4.43E-130	negative
DHX9	EXOSC10|647|ES	-0.62136	5.00E-116	negative
DHX9	COX15|12777|AT	-0.61875	8.49E-115	negative
DHX9	COX15|12776|AT	0.618747	8.51E-115	positive
DHX9	ZNF397|45145|AT	0.615491	2.80E-113	positive
DHX9	ASH1L|8088|ES	-0.61319	3.22E-112	negative
DHX9	ECT2|67659|ES	-0.63292	1.29E-121	negative
SNRNP70	RHOT2|32938|RI	0.655198	4.42E-133	positive
SNRNP70	ACTG1|44121|RI	0.617812	2.33E-114	positive
SNRNP70	CDK16|88911|AP	-0.61343	2.51E-112	negative
SNRNP70	C9orf117|87644|AT	0.695371	2.00E-156	positive
SNRNP70	RHBDF1|124991|AD	0.609376	1.78E-110	positive
SNRNP70	NRBP2|85507|RI	0.670627	1.30E-141	positive
SNRNP70	C9orf117|87643|AT	-0.68887	2.18E-152	negative
SNRNP70	PACS2|29630|AP	-0.68099	1.23E-147	negative
SNRNP70	CDC37|47514|RI	0.67433	9.76E-144	positive
SNRNP70	PACS2|29631|AP	0.625043	8.80E-118	positive
SNRNP70	TIPRL|8901|AT	-0.61651	9.47E-114	negative
SNRNP70	TIPRL|8902|AT	0.616499	9.54E-114	positive
SNRPA	GIT2|24375|AA	0.601304	7.18E-107	positive
SNRPA	SLC30A5|72303|AA	0.646812	1.19E-128	positive
GPATCH8	INPP5F|13276|RI	-0.60343	8.22E-108	negative
DDX3X	TUBGCP2|13527|AP	-0.63329	8.50E-122	negative
DDX3X	SYNJ2|78249|AD	-0.60375	5.96E-108	negative
DDX3X	INPP5F|13276|RI	-0.60152	5.77E-107	negative
DDX3X	LYRM5|20810|AT	-0.66132	2.10E-136	negative
DDX3X	LYRM5|20809|AT	0.661319	2.09E-136	positive
DDX3X	ATL2|53255|ES	-0.62583	3.69E-118	negative
DDX3X	EXOSC10|647|ES	-0.68049	2.44E-147	negative
DDX3X	COX15|12777|AT	-0.66833	2.60E-140	negative
DDX3X	COX15|12776|AT	0.668331	2.61E-140	positive
DDX3X	SLC30A5|72303|AA	-0.67253	1.06E-142	negative
DDX3X	ZNF397|45145|AT	0.621754	3.25E-116	positive
DDX3X	ASH1L|8088|ES	-0.66895	1.16E-140	negative
DDX3X	ABCC3|42464|RI	-0.60585	6.90E-109	negative

DDX3X	VPS13A|86650|AT	0.602355	2.47E-107	positive
CLK4	C9orf89|86903|RI	0.617241	4.30E-114	positive
ZFR	LYRM5|20810|AT	-0.62655	1.66E-118	negative
ZFR	LYRM5|20809|AT	0.626546	1.67E-118	positive
ZFR	ATL2|53255|ES	-0.61271	5.35E-112	negative
ZFR	EXOSC10|647|ES	-0.64151	6.38E-126	negative
ZFR	COX15|12777|AT	-0.61302	3.88E-112	negative
ZFR	COX15|12776|AT	0.613018	3.87E-112	positive
ZFR	ASH1L|8088|ES	-0.62624	2.35E-118	negative
SPEN	INPP5F|13276|RI	-0.60622	4.68E-109	negative
SPEN	LYRM5|20810|AT	-0.62152	4.18E-116	negative
SPEN	LYRM5|20809|AT	0.621527	4.17E-116	positive
SPEN	ASH1L|8088|ES	-0.63709	1.09E-123	negative
AGGF1	SUV420H1|17293|AT	-0.61571	2.22E-113	negative
AGGF1	SUV420H1|17294|AT	0.615709	2.22E-113	positive

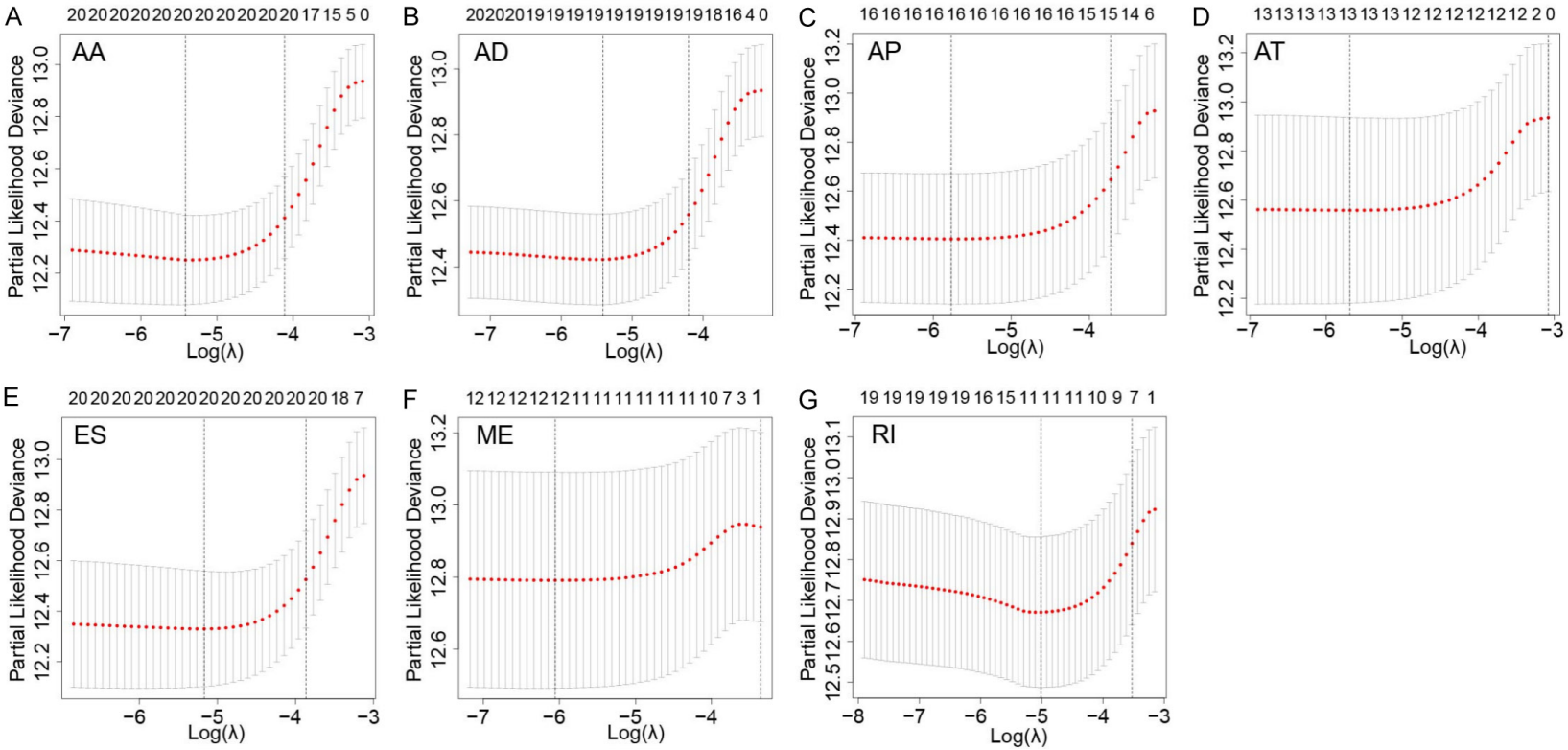

Figure S1. LASSO coefficient of survival-related AS events. (A) AA, (B) AD, (C) AP, (D) AT, (E) ES, (F) ME, and (G) RI events.

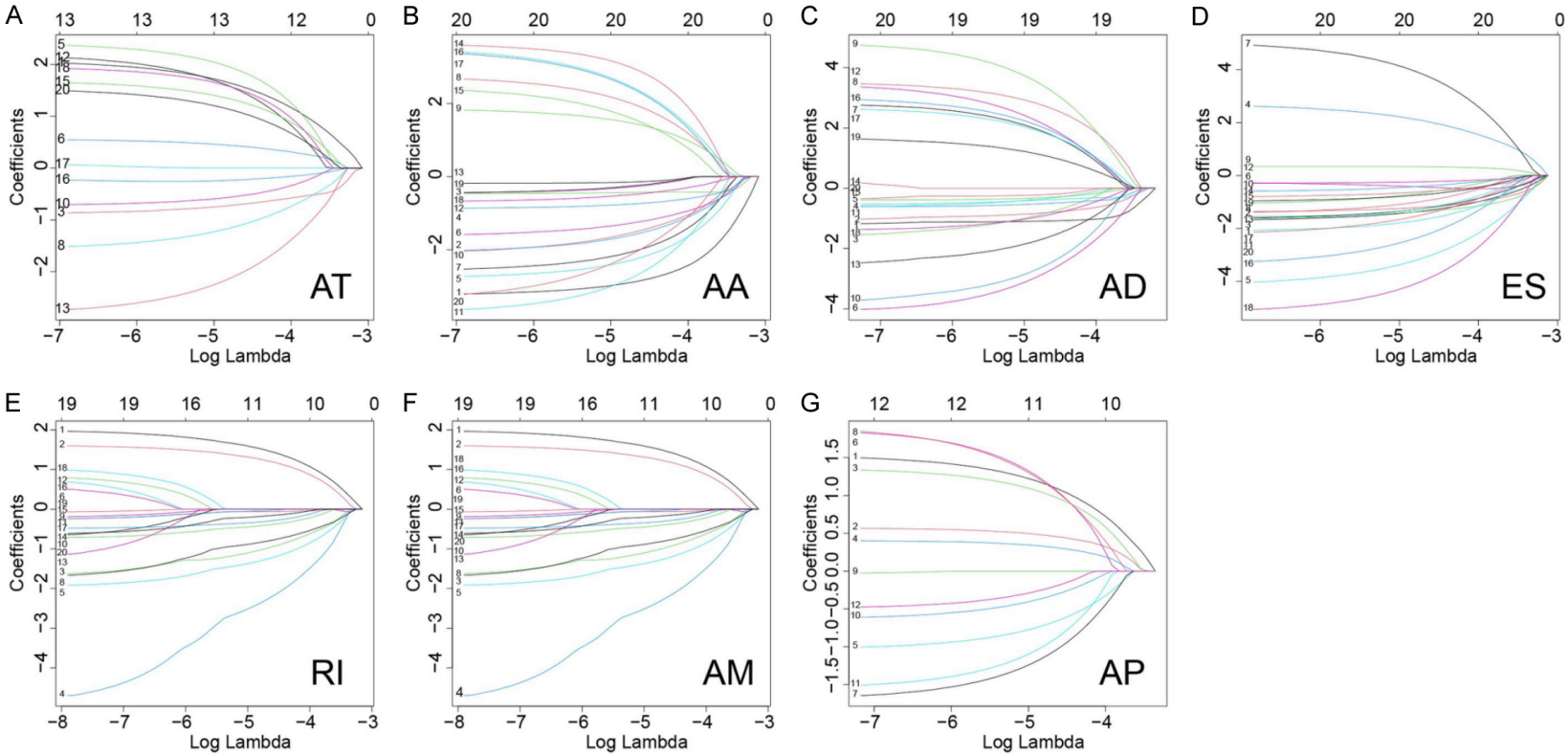

Figure S2. Error rate of cross-validation. (A) AA, (B) AD, (C) AP, (D) AT, (E) ES, (F) ME, and (G) RI events.

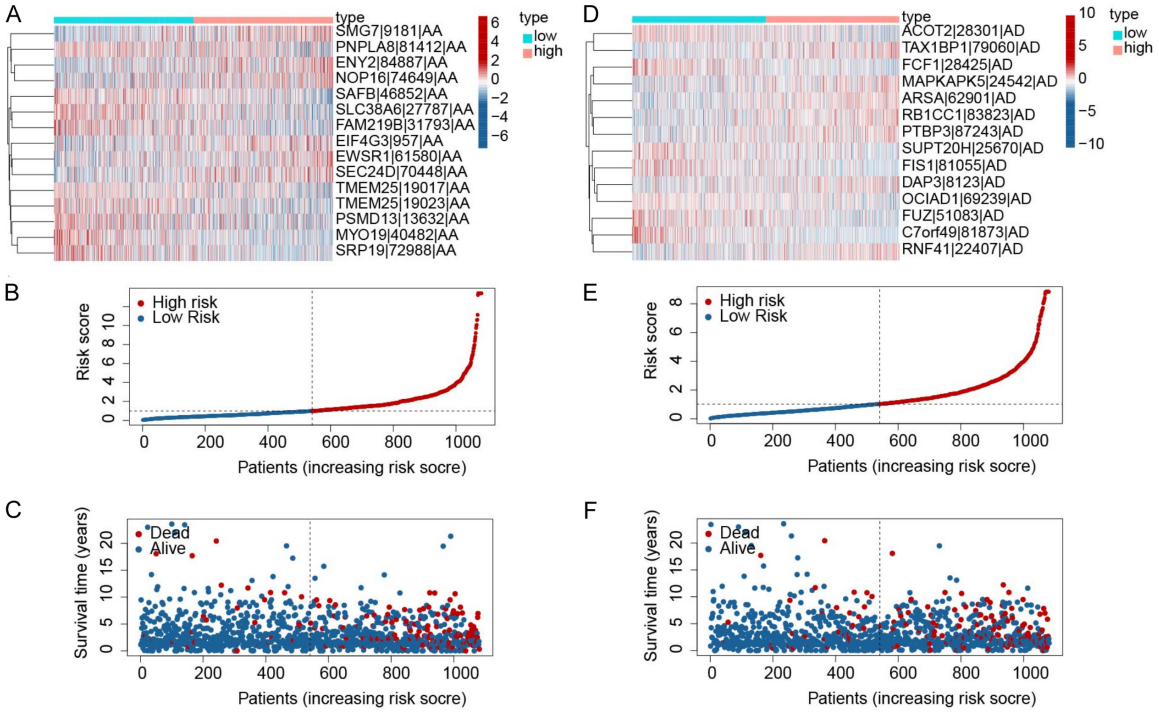

Figure S3. A. The heatmap of PSI values for AA events in BC. Red indicates high expression, and blue indicates low expression. B. The risk score distribution of the AA prognostic signature. C. The survival status and duration of patients with BC in the AA prognostic signature. D. The heatmap of PSI values for AD events in BC. Red indicates high expression, and blue indicates = low expression. E. The risk score distribution of the AD prognostic signature. F. The survival status and duration of patients with BC in the AD prognostic signature.

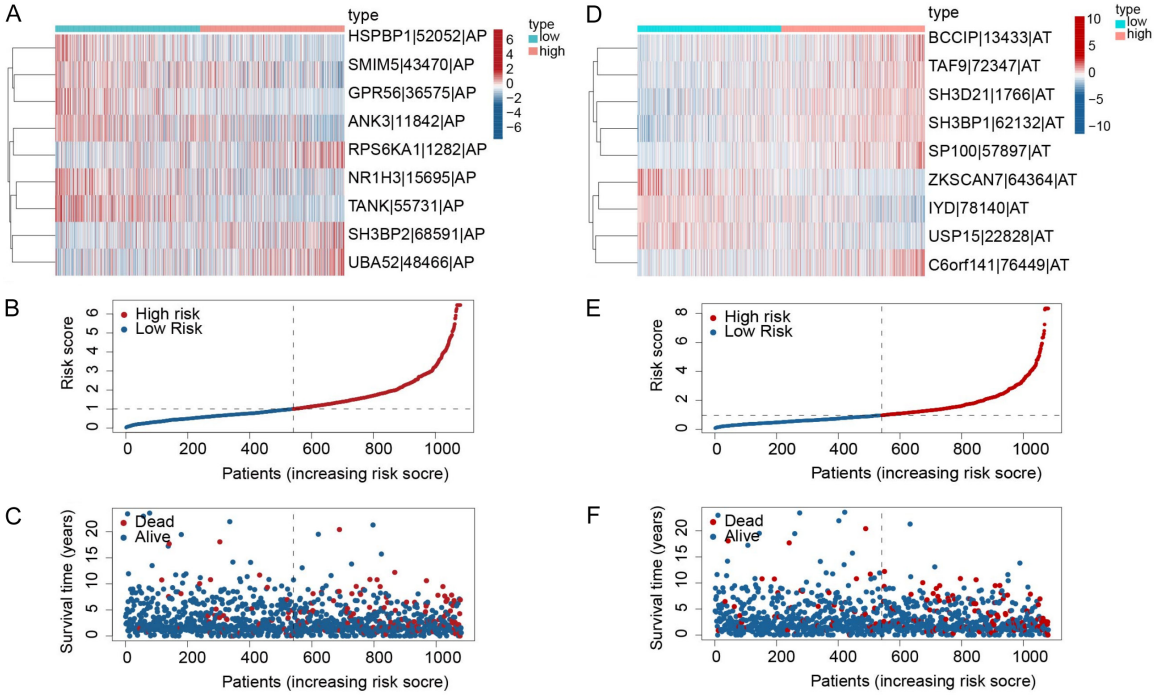

Figure S4. A. The heatmap of PSI values for AP events in BC. Red indicates high expression, and blue indicates low expression. B. The risk score distribution of the AP prognostic signature. C. The survival status and duration of patients with BC in the AP prognostic signature. D. The heatmap of PSI values for AT events in BC. Red indicates high expression, and blue indicate low expression. E. The risk score distribution of the AT prognostic signature. F. The survival status and duration of patients with BC in the AT prognostic signature.

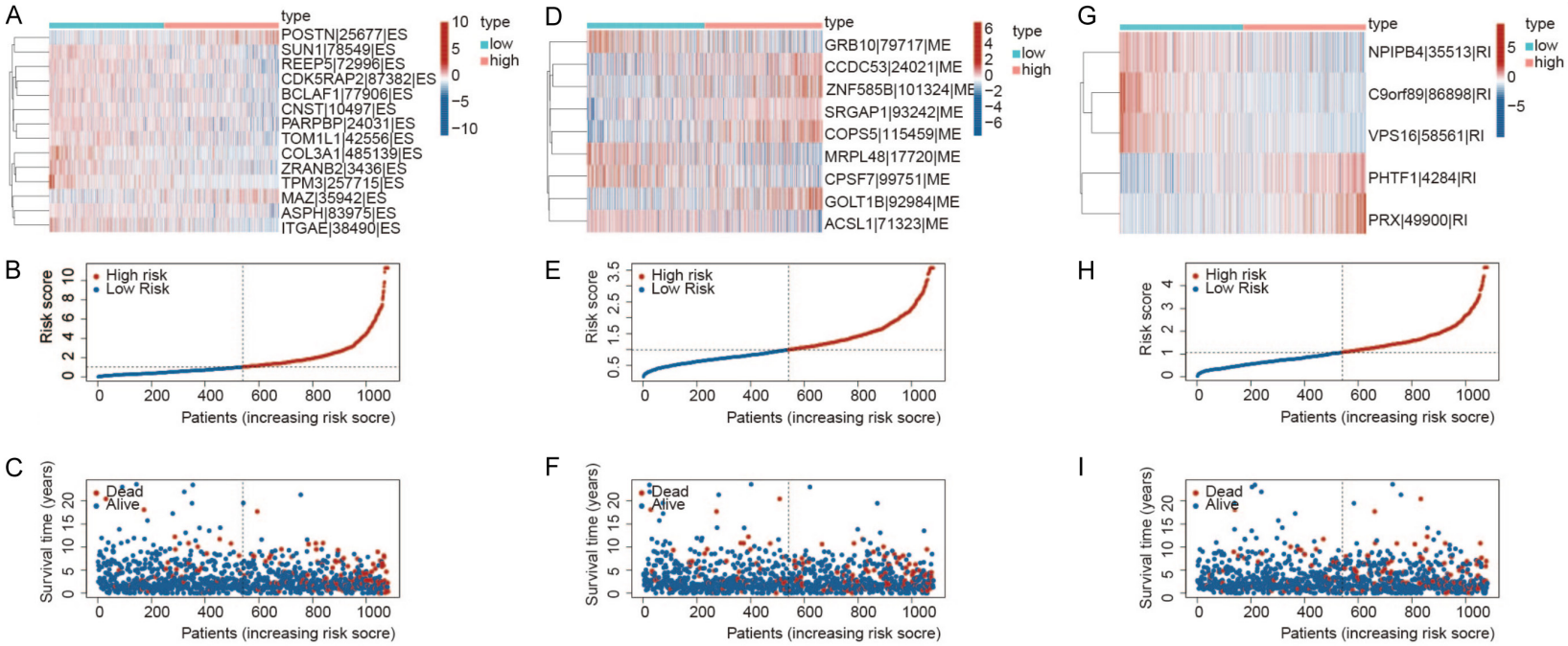

Figure S5. A. The heatmap of PSI values for ES events in BC. Red indicates high expression, and blue indicates low expression. B. The risk score distribution of the ES prognostic signature. C. The survival status and duration of patients with BC in the ES prognostic signature. D. The heatmap of PSI values for ME events in BC. Red indicates high expression, and blue indicates low expression. E. The risk score distribution of the ME prognostic signature. F. The survival status and duration of patients with BC in the ME prognostic signature. G. The heatmap of PSI values for RI events in BC. H. The risk score distribution of the RI prognostic signature. I. The survival status and duration of patients with BC in the RI prognostic signature.

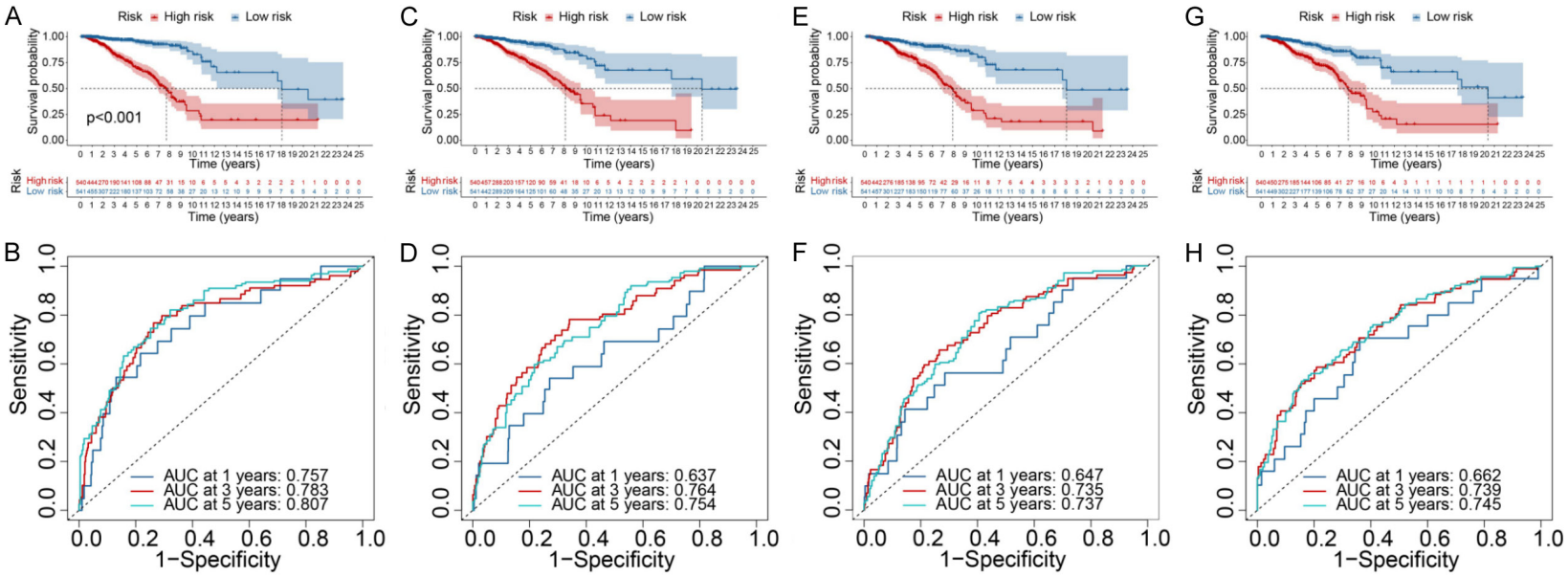

Figure S6. (A) Kaplan-Meier survival and (B) ROC analysis of the AA prognostic signature. (C) Kaplan-Meier survival and (D) ROC analysis of the AD prognostic signature. (E) Kaplan-Meier survival and (F) ROC analysis of the AP prognostic signature. (G) Kaplan-Meier survival and (H) ROC analysis of the AT prognostic signature.

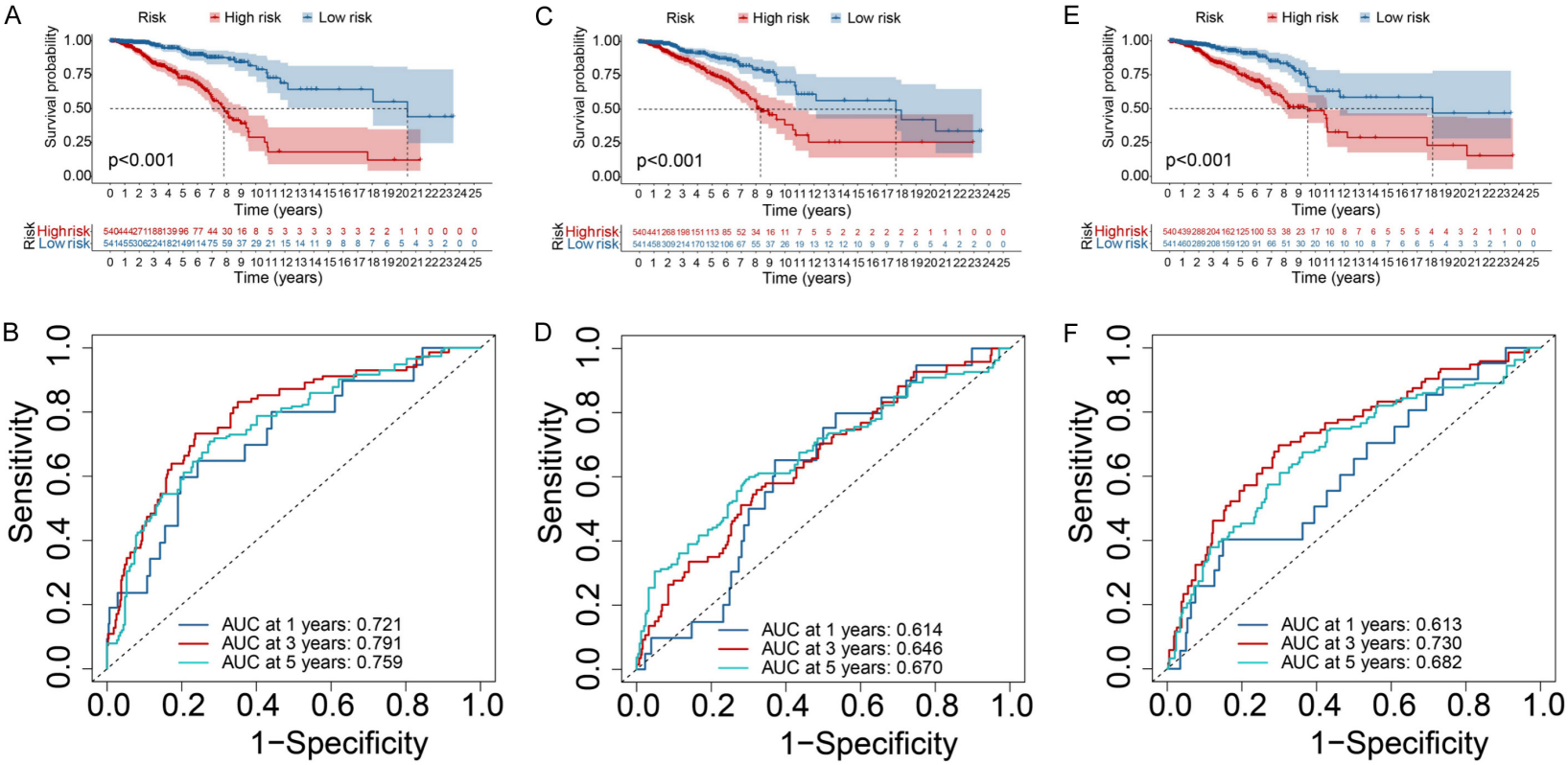

Figure S7. (A) Kaplan-Meier survival and (B) ROC analysis of the ES prognostic signature. (C) Kaplan-Meier survival and (D) ROC analysis of the ME prognostic signature. (E) Kaplan-Meier survival and (F) ROC analysis of the RI prognostic signature.

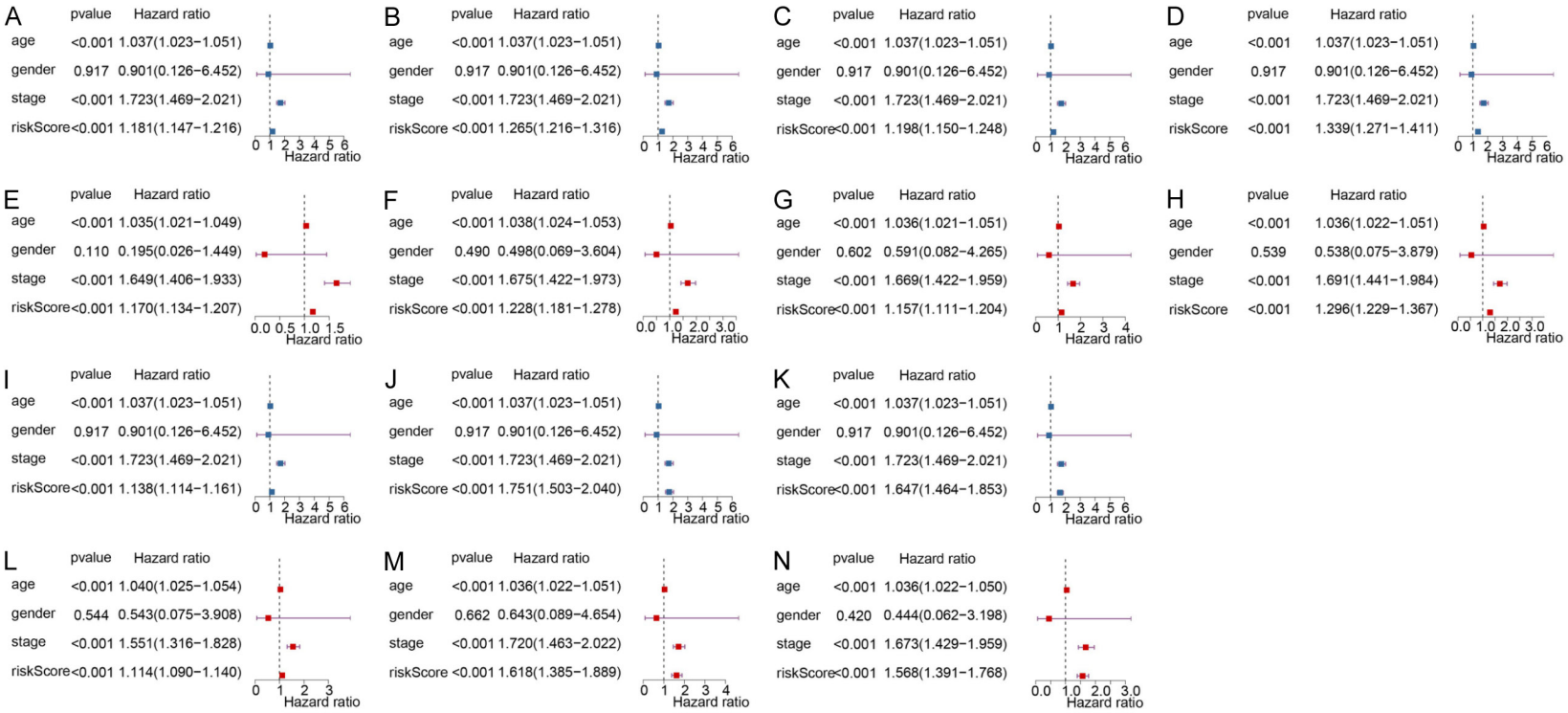

Figure S8. Univariate Cox regression analyses of (A) AA, (B) AD, (C) AP, and (D) AT prognostic signatures. Multivariate Cox regression analyses of (E) AA, (F) AD, (G) AP, and (H) AT prognostic signatures. Univariate Cox regression analyses of (I) ES, (J) ME, and (K) RI prognostic signatures. Multivariate Cox regression analyses of (L) ES, (M) ME, and (N) RI prognostic signatures.

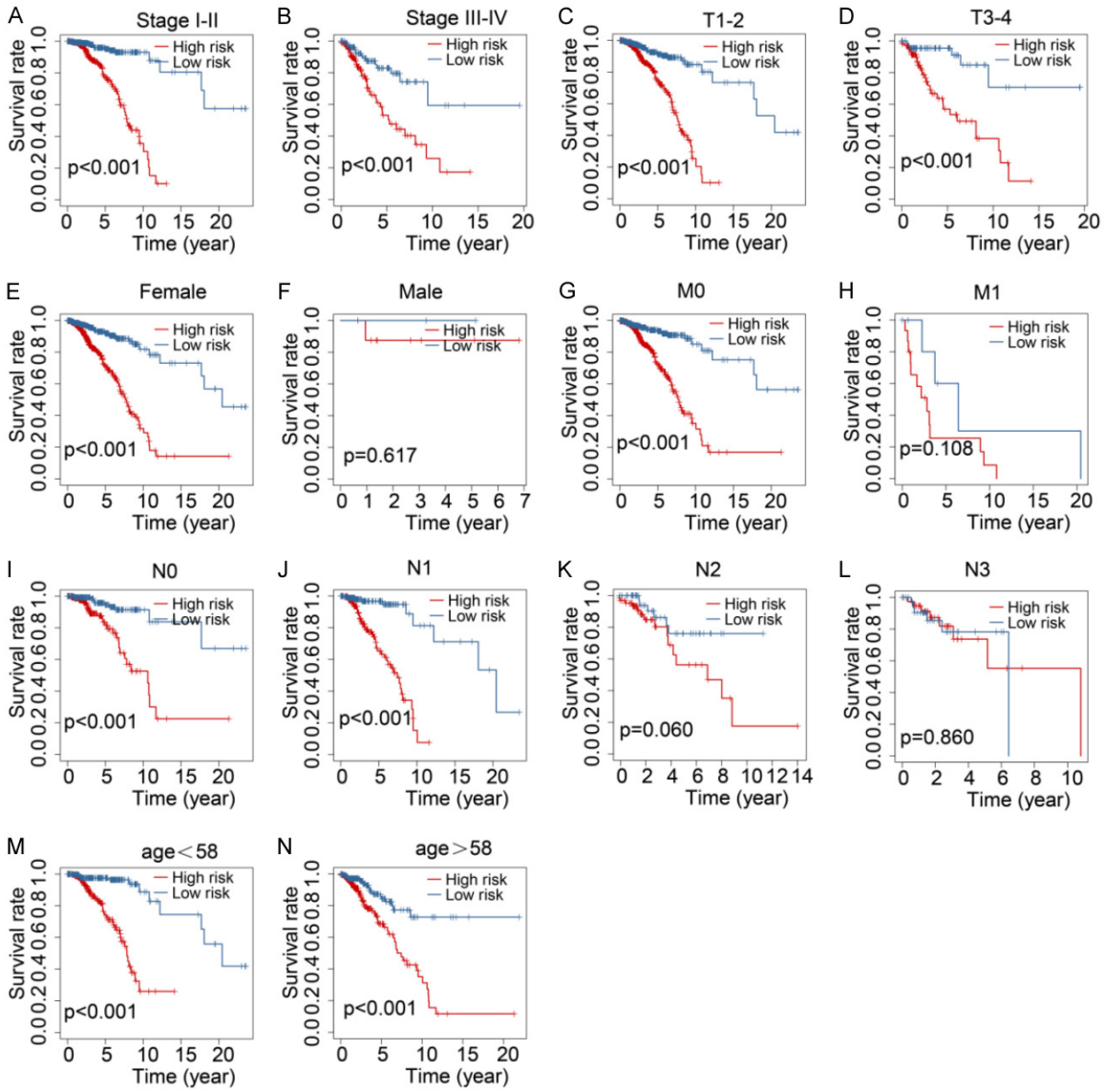

Figure S9. Kaplan-Meier survival analysis of the ALL signature in multiple BC subgroups stratified using the following clinical variables: (A, B) stage, (C, D) T status, (E, F) gender, (G, H) N status, (I-L) N status, and (M, N) age.

Table S4. Differential expression of genes related to prognosis of breast cancer

Gene	Con Mean	Treat Mean	Log FC	*P* Value
MAZ	3.317531	4.450483	1.132952	1.49E-53
PARPBP	0.638258	1.316934	0.678676	6.20E-44
PRX	1.904841	1.106393	-0.79845	7.10E-34
POSTN	5.388578	7.235761	1.847183	1.07E-32
ASPH	4.611379	3.641306	-0.97007	7.76E-22

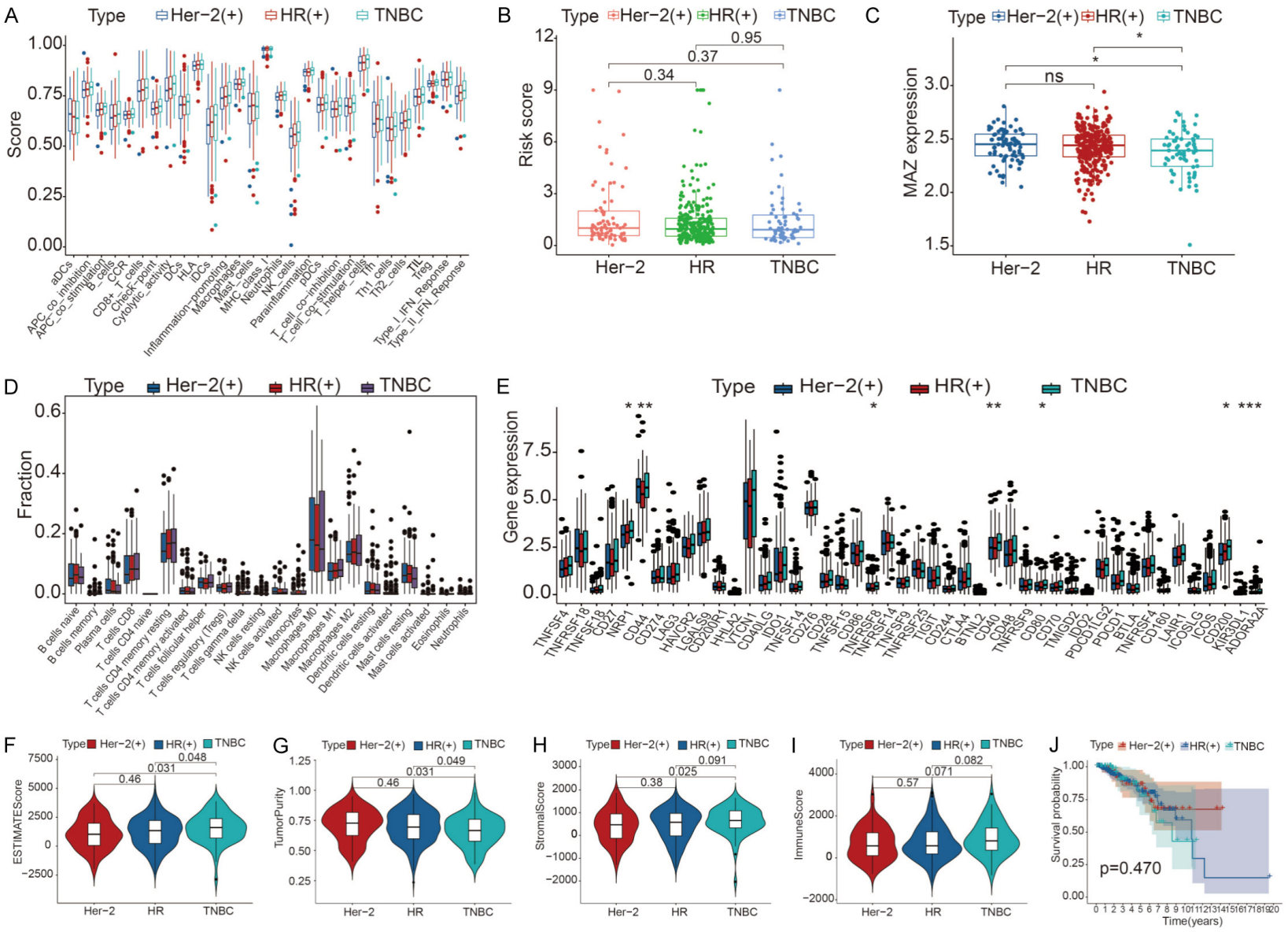

Figure S10. Subgroup analysis of BC with different molecular types. A. The distinction of enrichment of immune-related signatures in Her-2(+), HR(+), and TNBC groups. B. The correlation of risk score in Her-2(+), HR(+), and TNBC groups. C. MAZ expression in Her-2(+), HR(+), and TNBC groups. D. The difference in infiltrating immune cell subpopulations and levels among Her-2(+), HR(+), and TNBC groups. E. Comparison of expression levels of immune checkpoint blockade-related genes among Her-2(+), HR(+), and TNBC groups. F-I. Comparison of stromal, immune, and ESTIMATE scores and tumor purity among Her-2(+), HR(+), and TNBC groups. J. Comparison of survival probability among Her-2(+), HR(+), and TNBC groups.